*J. Fluid Mech.* (2019), *vol.* 868, *pp.* 385–427.  
doi:10.1017/jfm.2019.172

# Acoustic theory of the many-bladed contra-rotating propeller: analysis of the effects of blade sweep on wake interaction noise

**M. J. Kingan**[1] **and A. B. Parry**[2,†]

[1]Department of Mechanical Engineering, University of Auckland, Auckland 1010, New Zealand

[2]30 Ypres Road, Allestree, Derby DE22 2LZ, UK

(Received 20 July 2018; revised 4 December 2018; accepted 23 February 2019;
first published online 11 April 2019)

An analytical model is presented for the wake interaction tones produced by a contra-rotating propeller. We re-cast the usual far-field radiation formulae as a double integral over a nominal propeller source annulus. Assuming that the number of blades on both propellers is large, we evaluate the integral asymptotically in terms of its leading-order contributions from interior stationary or boundary critical points which represent the specific locations on the propeller annulus that dominate the sound radiation. The asymptotic approach is powerful producing results in the form of one-line algebraic formulae that contain no integrals or special functions yet remain accurate. The asymptotics show that sweep is not necessarily beneficial and can cause the blade design to become critical for particular tones and directions in terms of a continuum of interior points distributed along a line on the propeller source annulus producing a higher-order result and thus an enhanced radiated sound field. The paper also shows how the interior points are completely consistent with the sub- or super-critical gust response of a swept blade. Tones with low and zero azimuthal mode order are treated as special cases and the asymptotics show that, as the mode order reduces, the radiated sound becomes concentrated around the flight axis where even higher-order solutions are possible, including rings and annuli of stationary points around the propeller annulus. Full numerical calculations confirm the accuracy of the asymptotic approach.

**Key words:** aeroacoustics, wakes

## 1. Introduction

The noise of single-rotating propellers has been studied for many years. Apart from some early work by Lynam & Webb (1919) and Bryan (1920) the first complete description of propeller noise was given by Gutin (1936) and that of dual- and contra-rotating configurations by Hubbard (1948). We note, in passing, that early work on the strong effect of contra-rotation on axial flow fan noise was carried out by Young (1951) and Daly (1958). The propeller had a resurgence in the late 1970s and 1980s, due to high fuel prices, as a Prop-Fan concept which included a

† Email address for correspondence: anthony.parry.pig@gmail.com

single row of highly swept blades with large chord (see Rohrbach & Metzger 1975; Metzger & Rohrbach 1979), thus differing from the traditional propeller. General Electric added a second contra-rotating row and developed the un-ducted fan (UDF) which was flight tested (Harris & Cuthbertson 1987). (The idea of using sweep to increase propeller performance at high speed was not new; it had first been put forward by Brady (1951) but it was not pursued then because of the advent of the turbofan.) As fuel prices fell the concept was shelved. More recently, contra-rotating propellers have been considered, yet again, for next generation aircraft (see Fuss & Parry 2011), this time described as advanced open rotors, contra-rotating open rotors (CROR) or open fans. The main difference in the modern concept to that of the Prop-Fan is the increase in the number of blades. However, the fundamental physics of the aerodynamic interaction and noise radiation problem remains the same.

Modern advanced open rotor engines produce thrust via two contra-rotating, coaxial 'open rotors' (propellers) which are usually driven by a gas turbine housed within a large centrebody, which extends both fore and aft of the propellers. The downstream propeller is used to recover the swirl from the wake of the upstream propeller which significantly improves the efficiency relative to that of a single propeller engine.

It is well known that the propulsive efficiency of conventional turbofan engines can be improved by increasing the engine diameter and the bypass ratio. However, this approach is limited for turbofan engines by the corresponding increase in drag and weight associated with the nacelle as engine diameter increases. The lack of a shroud or outer nacelle on a propeller-driven engine means that the diameter of the propellers can be much larger than the fan of an equivalent turbofan engine. This larger diameter achieves the effect of a higher bypass ratio which results in a significant fuel efficiency improvement relative to current generation turbofan engines (Parker & Lathoud 2010).

The lack of a nacelle or shroud to shield and attenuate noise generated by the propeller blades means that there are clear challenges in the production of an open rotor design that generates an acceptable level of noise. Despite these challenges, model-scale tests of modern open rotors, along with the associated predictions, have shown that sufficiently quiet designs should be achievable (Fuss & Parry 2011; Parry & Vianello 2012).

The noise spectrum produced by the modern open rotor consists of a significant broadband level in addition to a multitude of tones (Parry, Kingan & Tester 2011). The tones include the usual 'rotor-alone' tones which occur at integer multiples of the blade passing frequency of each rotor as well as 'interaction' tones produced by the interaction of the blades with the unsteady flow-field from the adjacent propeller. At take-off and approach conditions, rotor-alone tones are primarily caused by the steady loading and thickness of the propeller blades as well as by the unsteady loading due to the flow distortions created by the pylon wake, the wing upwash and the non-uniform flow produced by the fuselage. Interaction tones are believed to be produced primarily by the periodic unsteady loading on the propeller blades with the unsteady loading on the downstream propeller blades caused by viscous wakes, tip vortices and bound potential fields from the upstream propeller. Noise is also generated on the upstream propeller blades due to their interaction with the bound potential field from the rear propeller. A discussion of the sources of these tones is given by Kingan *et al.* (2014). Note that modern open rotor designs have a 'cropped' downstream propeller (it has a smaller diameter than the upstream propeller) so that the interaction of the downstream propeller blades with the tip vortex from the upstream propeller is minimised (although it is important to note that account must be taken of incidence effects and streamtube contraction when the amount of 'crop' is determined).

In order to design an open rotor which produces an acceptable level of noise, suitable methods for noise prediction are required. There are a number of such methods available and a summary of many of these can be found in the review paper by the first author (Kingan 2014). As one might expect, these methods involve varying degrees of complexity and computational time and range from high fidelity, but time intensive, unsteady computational fluid dynamics (CFD) and computational aeroacoustics (CAA) methods to much faster analytical methods. It is not our intent here to give a detailed review of CFD/CAA methods for open rotors – as our focus is analytic and, particularly, asymptotic methods – but good examples in this area are Colin *et al.* (2012*a*,*b*), Colin, Caruelle & Parry (2012*c*), which discuss high- and low-fidelity noise prediction methods and show extensive comparisons of predictions with measured data, as well as Stürmer & Yin (2009), Peters & Spakovszky (2010), Zachariadis, Hall & Parry (2011), Brandvik, Hall & Parry (2012), Stürmer *et al.* (2012), Sharma & Chen (2013), Soulat *et al.* (2013, 2016), Falissard & Delattre (2014), Van Zante & Envia (2014), Delattre & Falissard (2015) and Sohoni *et al.* (2015). Although CFD/CAA methods are now commonly used for open rotor noise predictions, analytical models are still well suited for preliminary design studies that investigate the effect of different parameters on rotor noise, due to the short computational time required, because of the range of calculations that are needed at the early design stage and because of the absence of sufficient geometric or aerodynamic details for a higher fidelity calculation. Indeed, for a contra-rotating propeller – as the interaction tones decay only slowly with frequency – there can be very many interaction tones (potentially hundreds) across the audible frequency range; for each of these the radiated sound must be calculated multiple times to provide noise estimates at all possible observer locations: that is just for one operating point and for one design. At the early concept stage, therefore, when multiple architectures and designs are being considered, it remains the case that designers tend to rely on scaling rules or power laws. A simple algebraic expression describing how the sound level varies with propeller geometry, observer location and operating condition is therefore of great use as a design tool. Furthermore, analytical methods are able to produce insights into the noise generation and propagation phenomena that are not readily available via other approaches. Of course, as a practical design evolved, and more detailed geometries became available, the fidelity of the method used for calculations would naturally increase.

For the purposes of analytical modelling, the unsteady flow-field produced by each propeller blade can be decomposed into (i) the viscous wake, (ii) the tip vortex and (iii) the bound potential field. The velocity perturbation associated with each of these fields can then be decomposed into a Fourier series of 'harmonic gusts' by making use of the periodicity of the problem in the azimuthal coordinate (the angle through which the blade rotates). The unsteady loading on or 'response' of the adjacent propeller's blades to the each of these gusts is then calculated using well-known 'blade response functions'. Analytical models for the viscous wake and bound potential field sources are described in Parry (1988, 1997) and Parry & Crighton (1989*a*). Recently there has been a number of models developed for predicting the unsteady field produced by the tip vortex and the resulting unsteady loading on the downstream propeller blades and acoustic radiation e.g. Kingan & Self (2009), Roger, Schram & Moreau (2012, 2014), Moreau, Quaglia & Fernando (2015), Jaouani *et al.* (2016) and Quaglia *et al.* (2016, 2017). In particular, Quaglia *et al.* (2017) presents an advanced analytical model which takes streamtube contraction into account.

Carazo, Roger & Omais (2011) present an analytical framework for the prediction of open rotor noise similar to that presented here. Wake profiles were modelled either

using a simple analytical model (as it the case here) or were taken directly from CFD simulations. Blade response was calculated using a method similar to those described in Roger & Carazo (2010) who extend the analytical model of Adamczyk (1974) for calculating the high-frequency response of a swept flat plate blade to a convected harmonic gust by including the effect of both swept leading and trailing edges and even the blade tip. Unlike the method presented here, Carazo *et al.* decompose the unsteady flow field from the upstream propeller into an azimuthal and radial sum of Fourier harmonics. This approach results in a double summation of convected harmonic gusts which interact with the downstream blade row producing unsteady loading. In this paper we use only an azimuthal decomposition and use a 'local' method to account for the sweep of the blade leading edge relative to the gust. Grasso *et al.* (2014) have also developed an analytical method for predicting noise from a contra-rotating fan which is similar to that of Carazo *et al.*

The far-field radiation can be calculated from the unsteady loading using the analytic 'frequency domain' solutions of Hanson (1985) and Parry (1988) (which are similar to the radiation formulae used by Carazo *et al.* and Grasso *et al.*). However, these methods involve, for each individual tone, a double integration over the blade planform area (chord and span) for which at least one integral must be evaluated numerically. (Other, more advanced, frequency domain methods (e.g. Hanson & Parzych 1993) have been developed for predicting unsteady loading noise from a propeller where the integration is over the actual blade surface. Because the blades of a modern advanced open rotor are very thin, the approach of Hanson (1985) and Parry (1988), where the integration is over the blade chord line instead, is a reasonable approximation. However, the assumption that the blades are aligned with the local mean flow and wake swirl and induced axial velocity can be neglected, which is implied in these methods, can introduce errors. As the purpose of this paper is to demonstrate the asymptotic approach, rather than to present a state-of-the-art, high-fidelity noise prediction method, acoustic radiation is calculated using the approach of Hanson (1985) and Parry (1988).) Furthermore, the integrals involve Bessel functions and complex phase terms. In order to provide a faster and more insightful solution, Parry & Crighton (1989*b*) and Crighton & Parry (1991, 1992), considering the rotor-alone tones, showed how the Bessel functions and the radial integral could be removed entirely by assuming that the number of blades was large (an assumption that is quite reasonable on modern propellers) and then evaluating both the Bessel function and the radial integral asymptotically. The approach showed how the noise is completely governed by the tip for a subsonic propeller, and by the sonic radius for a supersonic propeller. For both of these cases, the asymptotic approach produced a closed form, algebraic result which was accurate and showed how the noise was related to the geometry and aerodynamics of a particular propeller radius. Parry (1988) and Parry & Crighton (1989*a*) also extended this one-dimensional asymptotic analysis to interaction noise. The role of quadrupole effects in propeller radiation was discussed by Peake & Crighton (1991*a*) and the extension of the asymptotic approach for single-rotating propellers to include near-field noise radiation was addressed by Peake & Crighton (1991*b*) and applied by Peake & Boyd (1993).

One of the important blade design features used to control open rotor noise is blade sweep. Parry (1995) extended previous work to supersonic single-rotating propellers with sweep by using two-dimensional asymptotics over the nominal propeller annulus where, once again, the blade number was assumed to be the large parameter. The approach showed precisely how and where on the annulus the dominant noise sources were generated and, moreover, that sweep was not always beneficial. Indeed, it showed

that there was a 'critical sweep design' that was significantly noisier than a straight-bladed propeller.

An alternative to the analytical/semi-numerical approach is a hybrid method that uses high-fidelity aerodynamic flow calculations, coupled to a high blade count asymptotic approximation of the Ffowcs Williams–Hawkings (FW-H) equation and such an approach was considered by Envia (1994) for single-rotating propellers and, more recently, extended (Envia 2015) for contra-rotating open rotors. The advantages of the hybrid approach are that the solution can be used in either the near-field or the far-field, and that the quadrupole terms can be included naturally in the calculation. However, that approach is not as suited to early conceptual and preliminary design studies as that described here because there is still a computational overhead involved in the flow calculation and, moreover, the detailed blade geometries are not generally available at the early design stage.

In this paper we extend the asymptotic approach of Parry (1995) considerably: first of all for application to contra-rotating propeller interaction noise; and secondly, to incorporate the effects of both sweep and lean. We show how the asymptotic approach can be used to help understand where the noise is generated. The essential asymptotic assumption is that the blade numbers of both front and rear propellers are large. The resultant far-field sound pressure produced by the interaction tones is in the form of a double integral over a 'propeller source annulus'. The general form of the integrand is $G(z)\exp\{\mathrm{i}\nu\Phi(u,z)\}$ where $G(z)$ is an amplitude function dependent on non-dimensional radii, $z$, only, $\nu$ is the azimuthal mode order of the tone and $\Phi(u,z)$ is a phase function which is dependent on $z$ and the azimuthal angle on the source annulus $u$. For tones where $|\nu|$ becomes large, the integrand becomes highly oscillatory and the integral may be evaluated using asymptotic methods for double integrals.

The amplitude function $G(z)$ includes the effect of the unsteady aerodynamic response of the rear row to the incoming wakes. The blade response itself is affected by the blade sweep and, for a consistent calculation, the oblique nature of the gust interaction must be included. The effect of sweep on blade response was studied analytically by Graham (1970) and Adamczyk (1974) who considered an infinite span aerofoil and Envia & Kerschen (1984, 1986) who studied interactions with a stator vane. The effects of both sweep and lean on rotor–stator interaction were considered by Envia & Kerschen (1990), Glegg (1999) and Cooper & Peake (2005, 2006). Additional studies were undertaken by Hanson (2001) who adapted Glegg's (1999) work on interaction tones for application to broadband noise from ducted rotors. These studies showed that the response can switch from super-critical to sub-critical for particular combinations of sweep and Mach number (and also lean). The phrases super- or sub-critical response imply supersonic or subsonic leading-edge trace velocity and, for two-dimensional sound radiation calculations, they lead to propagating and evanescent sound fields, respectively. Here we apply previous quasi-three-dimensional results to determine the relevant gust response function – after a suitable coordinate transformation – for both super-critical and sub-critical aerodynamic interactions showing clearly the point (in terms of sweep angle and Mach number) at which the nature of the response changes. We also demonstrate that, to leading order, the resultant magnitude of $G(z)$ – including the effects of oblique incidence – is unaffected by the super- or sub-critical nature of the response.

De Laborderie & Moreau (2016) presented an analytical model for predicting the tones produced by the rotor–stator interactions in a ducted fan. The model is similar in principle to that presented here: rotor wakes are modelled or measured and then

decomposed into a sum of harmonic gusts. The response of the stator blades to these gusts is predicted using a blade response function. The radiated acoustic field is then predicted using an acoustic analogy. The method is used to conduct a parametric study investigating the effects of stator sweep and lean on radiated noise levels. Zhang *et al.* (2017) conducted a similar study investigating the effect of stator sweep and lean on fan tone and broadband interaction noise levels using an analytical model.

We start in § 2 with the specification of the framework for the full numerical solution. In § 2.1, the generic unsteady velocity fields, produced by the $B_1$ upstream blades, are defined and then convected by the flow towards the $B_2$-bladed rear row of the propeller. The velocity field is written in Fourier form in a frame of reference locked to the rear row. For the unsteady aerodynamics, a coordinate transformation is derived in § 2.2 that switches from a wake–blade row interaction to an equivalent interaction of a wake with a swept aerofoil, enabling us to use Adamczyk's (1974) response function. The acoustic radiation integrals are quoted in § 2.3, incorporating the unsteady lift coefficients from § 2.2.

In § 3 we evaluate the radiation double integral asymptotically in terms of the principle contributions arising from small regions of the integrand around certain 'critical points'. These critical points can be divided into two different types: interior stationary points, which occur within the source annulus (or on the annulus boundary) at locations corresponding to the stationary points of the phase function, or boundary critical points which, as their name suggests, only occur on the source annulus boundary and occur at locations where only the tangential derivative of the phase function vanishes. The asymptotic theory indicates that as $|\nu| \to \infty$ the radiated tone amplitude, where the leading-order contributions are due to interior stationary points, are significantly higher than those where the leading-order contributions are due to boundary critical points.

In § 4 we discuss the implications of the asymptotic analysis for blade sweep. In particular, a discussion is given in § 4.1 of the link between the interior stationary points and the super- or sub-critical nature of the unsteady response of the downstream swept blades to the incident wakes where we show that interior stationary points cannot exist at radii for which the blade response is sub-critical. We also note that a 'critical blade design' can be conceived for which interior stationary points exist as a continuum along the blade span. The asymptotic solution for such a design is derived in § 4.2.

For completeness, in § 5, we also address cases in which $|\nu|$ is no longer large. Specifically, we consider $|\nu| = O(1)$ in § 5.1 and $\nu = 0$ in § 5.2 with the blade numbers remaining large in both cases. Here there are some subtle differences in the asymptotics, for which we introduce the non-dimensional frequency term $\eta$ that is of the same order as the blade numbers.

In § 6 we compare the asymptotic results with full numerical calculations for two realistic cases, one straight-bladed and one with leading-edge sweep in order to discover, first, whether tones for which the leading-order contribution is caused by an interior stationary point are, indeed, higher in level than those for which the leading-order contribution is due to a boundary critical point and, second, what the differences are in the results for straight and swept-blade configurations in terms of amplitude and the angular range over which the sound field is dominated by interior stationary point contributions.

## 2. Formulation of full numerical solution

In this section a model is presented for calculating the tonal noise produced by the unsteady loading on the downstream propeller blades due to their interaction with

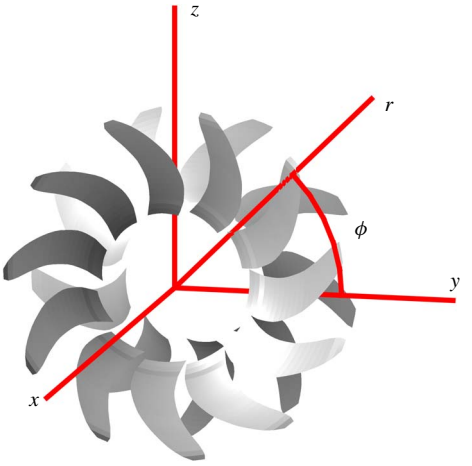


FIGURE 1. (Colour online) Contra-rotating propeller blades and coordinates.

the wakes from the upstream propeller. For the analysis presented in this paper, it will be convenient – and consistent with the work of Hanson (1985) – to introduce a cylindrical coordinate system, $\{x, r, \phi\}$, where $x$ is the axial coordinate which is directed upstream and is co-linear with the propeller axis, $r$ is the radial coordinate and $\phi$ is the azimuthal angle. This coordinate system is shown in figure 1. The propellers are immersed in a uniform airflow with Mach number $M_x$ in the negative $x$-direction relative to the engine and the air has ambient density $\rho_0$ and speed of sound $c_0$. The upstream and downstream propellers rotate in the negative and positive $\phi$-directions at rotational speeds $\Omega_1$ and $\Omega_2$ respectively. The pitch-change axes of the reference blades on the front and rear propellers are located at $\phi = 0$ at time $\tau = 0$ and are separated by a distance $g$ in the axial direction. Also note that the convention adopted in this paper will be that the subscripts 1 and 2 respectively denote parameters associated with the upstream and downstream propellers. The blades of both propellers have chord $c(r)$ and sweep $s(r)$ and both propellers have $B$ blades and the downstream propeller has a diameter which is denoted $D$. Blade sweep is defined, as in Parry (1988), as the distance by which the blade mid-chord is offset from the pitch-change axis in the helical direction aligned with the local flow (see figure 2).

In what follows, it will be necessary to introduce a number of different coordinate systems to be applied at each local radial station $z$. For the front row we must account for the relative motion of the blades and also the direction of wake convection. For the rear row, we must account for the relative motion of the blades (in the opposite direction) and the blade stagger angle. A transformation is also required to re-orient the radial direction so that it is aligned, locally, with the rear blade's leading edge to account for the effects of leading-edge sweep. These transformations were referred to in § 1 and are discussed in more detail in §§ 2.1 and 2.2 below but we emphasise the importance of them again here as they are essential to the analysis in order to ensure that we account for changes in frequency with frame of reference, that we can apply standard quasi-two-dimensional gust response theory and – most importantly – that we properly account for the phase of the resultant unsteady loading on the rear row blades that will drive the acoustic radiation. A precise description of the phase is absolutely essential for the asymptotic analysis that will follow in § 3.

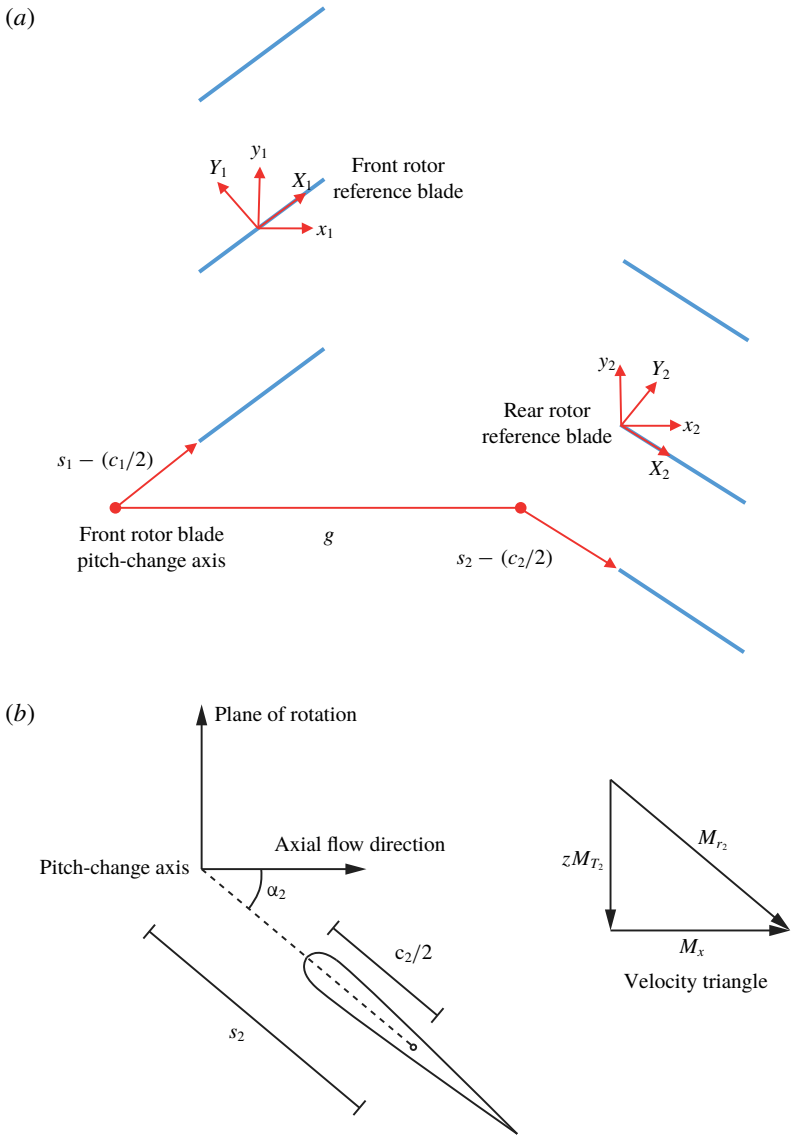


FIGURE 2. (Colour online) Schematic of the equivalent two-dimensional cascade problem (*a*). Sweep definition (*b*).

### 2.1. *Unsteady velocity fields*

The unsteady loading on the downstream propeller blades at a given radial location is calculated using an equivalent two-dimensional problem where the wakes from an upstream cascade of blades interact with the blades of a downstream cascade. This situation is illustrated in figure 2. The formulation presented here will make use of a Cartesian coordinate system $\{x_1, y_1\}$, where $x_1$ is an axial coordinate defined such that the airflow has Mach number $M_x$ in the positive $x_1$-direction and $y_1$ is a tangential coordinate which is parallel to the direction in which the blade rows translate. Note that, as the models for wake convection and rear rotor unsteady response follow the

usual conventions, the $x_i$-axes are directed downstream, unlike the cylindrical polar system shown in figure 1 in which the $x$-axis is directed upstream. The upstream and downstream blades translate in the negative and positive $y$-directions at Mach numbers $\Omega_1 r/c_0$ and $\Omega_2 r/c_0$ respectively. At time $\tau = 0$ the pitch-change axis of the front propeller reference blade is aligned with the pitch-change axis of the rear propeller reference blade at $y_1/D = 0$ and the spacing between the mid-chord positions of the blades on each cascade in the $y_1$-direction is equal to $2\pi r/B$. The blades are modelled as infinitely thin flat plates which are aligned with the local flow direction but otherwise have identical characteristics (chord length, sweep, lean and drag coefficient) to the actual propeller blade at that particular radius. Also, the effect of the flow induced by the propellers is neglected such that the stagger angle, $\alpha$, of each blade is defined by $\tan\alpha = zM_T/M_x$, where $z = 2r/D$ and $M_T = \Omega D/2c_0$. The Mach number of the flow relative to each blade is denoted $M_r$. These assumptions are entirely consistent with Hanson's helicoidal surface theory (1983, 1985) for both single- and contra-rotating propellers which forms the basis for the acoustic radiation calculations in § 2.3.

In order to describe the development of the wakes from the upstream cascade it is convenient to introduce two coordinate systems which are locked to the upstream blade row and have origins located at the mid-chord of the upstream reference blade. The $\{x_1, y_1\}$ coordinate system has coordinates which are parallel to the global $\{x, y\}$ coordinate system. The $\{X_1, Y_1\}$ coordinate system has coordinates parallel to the chordwise and chord-normal directions and is related to the $\{x_1, y_1\}$ coordinate system by

$$X_1 = x_1 \cos\alpha_1 + y_1 \sin\alpha_1, \tag{2.1}$$

$$Y_1 = -x_1 \sin\alpha_1 + y_1 \cos\alpha_1. \tag{2.2}$$

The velocity deficit from the upstream reference blade is taken to be completely general and is denoted as the vector $\overline{\boldsymbol{u}}'(x_1, y_1)$. Note that this deficit velocity is most naturally expressed in the $\{X_1, Y_1\}$ coordinate system as, following our assumption that the blade has no thickness and does not turn the flow, the wake centreline remains aligned with the $X_1$ coordinate. The upstream propeller blades are assumed to be evenly spaced and identical and thus the mean velocity deficit produced by the upstream cascade, $\overline{\boldsymbol{v}}'$, is given by

$$\overline{\boldsymbol{v}}' = \sum_{n_1=-\infty}^{\infty} \overline{\boldsymbol{u}}' \left( x_1, y_1 + \frac{2\pi r}{B_1} n_1 \right). \tag{2.3}$$

In order to calculate the response of the downstream blade row, the wakes are assumed to be frozen in the vicinity of the leading edge of the downstream blade row. Applying Poisson's summation theorem to (2.3), the velocity deficit incident on the downstream blade row is given as a sum of Fourier harmonics by

$$\overline{\boldsymbol{v}}' = \sum_{n_1=-\infty}^{\infty} \boldsymbol{u}_{n_1} \exp\left\{ \mathrm{i}\frac{n_1 B_1}{r} y_1 - \mathrm{i}\frac{n_1 B_1}{r} x_1 \tan\alpha_1 \right\}, \tag{2.4}$$

where

$$\boldsymbol{u}_{n_1} = \frac{B_1}{2\pi r} \int_{-\infty}^{\infty} \overline{\boldsymbol{u}}'(x_1, y_c + x_1 \tan\alpha_1) \exp\left\{ -\mathrm{i}\frac{n_1 B_1}{r} y_c \right\} \mathrm{d}y_c, \tag{2.5}$$

and we have used the translated coordinate $y_c = y_1 - x_1 \tan\alpha_1$ to centre the Fourier integral on the wake centreline.

In order to calculate the unsteady loading on the downstream blade row, it is necessary to express $\overline{\boldsymbol{v}}'$ in a coordinate system fixed to the rear propeller blades. For this purpose we introduce a blade locked axial/tangential coordinate system $\{x_2, y_2\}$ which is parallel to the $\{x_1, y_1\}$ coordinates and has an origin located at the leading edge of the reference blade on the downstream blade row. The $\{x_2, y_2\}$ coordinate system is related to the $\{x_1, y_1\}$ coordinate system by

$$x_1 = x_2 + g - s_1\cos\alpha_1 + \left(s_2 - \frac{c_2}{2}\right)\cos\alpha_2, \tag{2.6}$$

$$y_1 = y_2 + (\Omega_1 + \Omega_2)r\tau - s_1\sin\alpha_1 - \left(s_2 - \frac{c_2}{2}\right)\sin\alpha_2. \tag{2.7}$$

One final coordinate transformation is required in order to express $\overline{\boldsymbol{v}}'$ in terms of the chordwise/chord-normal coordinate system of the downstream reference blade, $\{X_2, Y_2\}$, which is defined by

$$x_2 = X_2\cos\alpha_2 + Y_2\sin\alpha_2, \tag{2.8}$$

$$y_2 = -X_2\sin\alpha_2 + Y_2\cos\alpha_2. \tag{2.9}$$

Using (2.6)–(2.9) in (2.4) enables the (arbitrary) velocity deficit from the $B_1$ front row blades to be expressed in the $\{X_2, Y_2\}$ coordinate system as

$$\overline{\boldsymbol{v}}' = \sum_{n_1=-\infty}^{\infty} \boldsymbol{u}_{n_1} \exp\left\{\mathrm{i}n_1B_1(\Omega_1+\Omega_2)\tau - \mathrm{i}k_X X_2 - \mathrm{i}k_Y Y_2 - \mathrm{i}k_X\left(s_2 - \frac{c_2}{2}\right) - \mathrm{i}k_{Y_1} g\sin\alpha_1\right\}, \tag{2.10}$$

where the wavenumbers $k_X$, $k_Y$ and $k_{Y_1}$ are defined as

$$k_X = \frac{n_1B_1}{r\cos\alpha_1}\sin(\alpha_1+\alpha_2) = \frac{2n_1B_1}{DM_{r_2}}[M_{T_1} + M_{T_2}], \tag{2.11}$$

$$k_Y = -\frac{n_1B_1}{r\cos\alpha_1}\cos(\alpha_1+\alpha_2) = -\frac{2n_1B_1}{DM_{r_2}}\left[\frac{M_x}{z} - z\frac{M_{T_1}M_{T_2}}{M_x}\right], \tag{2.12}$$

and

$$k_{Y_1} = \frac{n_1B_1}{r\cos\alpha_1} = \frac{2n_1B_1M_{r_1}}{zDM_x}. \tag{2.13}$$

The mean upwash velocity (which is the component of velocity normal to the rear row blades, or in the $Y_2$ direction) onto the downstream reference blade is given by $w = \boldsymbol{j}_{Y_2}\cdot\overline{\boldsymbol{v}}'$, where $\boldsymbol{j}_{Y_2}$ is a unit vector aligned with the $Y_2$ coordinate. The upwash at the chord line of the reference blade of the downstream blade row (on which $Y_2 = 0$) is thus equal to a sum of convected harmonic gusts

$$w = \sum_{n_1=-\infty}^{\infty} w_{n_1}\exp\{\mathrm{i}k_X(U_{r_2}\tau - X_2) - \mathrm{i}k_Y Y_2\}, \tag{2.14}$$

where $U_{r_2}$ is the velocity magnitude of the air relative to the downstream blade and

$$w_{n_1} = \hat{w}_{n_1}\exp\left\{-\mathrm{i}k_X\left(s_2 - \frac{c_2}{2}\right) - \mathrm{i}k_{Y_1}g\sin\alpha_1\right\}, \tag{2.15}$$

with $\hat{w}_{n_1} = \boldsymbol{j}_{Y_2}\cdot\boldsymbol{u}_{n_1}$.

The total unsteady lift force per unit area acting on the chord line of the reference blade can be expressed as the sum of the unsteady 'response' of the blade to all of the upwash harmonics i.e.

$$\Delta p(\overline{X}_2) = \sum_{n_1=-\infty}^{\infty} \Delta p_{n_1}(\overline{X}_2) \exp\{\mathrm{i}n_1 B_1(\Omega_1 + \Omega_2)\tau\}, \tag{2.16}$$

where $\Delta p_{n_1}(\overline{X}_2) \exp\{\mathrm{i}n_1 B_1(\Omega_1 + \Omega_2)\tau\}$ is the response of the reference blade to a gust of the form $w_{n_1} \exp\{\mathrm{i}k_X(U_{r_2}\tau - X_2) - \mathrm{i}k_Y Y_2\}$ and $\Delta p_{n_1}$ can be expressed in the form

$$\Delta p_{n_1}(\overline{X}_2) = 2\pi\rho_0 U_{r_2} w_{n_1} \mathbb{S}(\sigma_2, M_{r_2}, \overline{X}_2, \Lambda), \tag{2.17}$$

where $\overline{X}_2 = 2X_2/c_2$ is a dimensionless chordwise coordinate, $\sigma_2 = k_X c_2/2$ is the reduced frequency, $\Lambda$ is a local blade leading-edge sweep angle (defined in the following section) and $\mathbb{S}$ is a non-dimensional response function.

### 2.2. *Unsteady aerodynamic response*

In § 2.1, above, we considered the aerodynamics of a purely two-dimensional cascade of blades in terms of the wake flows from the upstream blades. However, for the unsteady response of the downstream blades it is important that we account for the local three-dimensional response that occurs when the rear blades are swept. Our model for the propellers follows the helicoidal blade approach of Hanson (1983) so that there is no wake swirl and, consequently, our consideration of oblique incidence is restricted solely to blade sweep effects.

We consider an infinitely small blade element of spanwise length $\mathrm{d}z_2$ at radial location $z_2$ where $z_2 = 2r/D$ is the normalised radius of the rear row. Since, in this paper, the aerodynamics is considered to be quasi-two-dimensional, we must 'unwrap' and 'untwist' the blades to produce an equivalent interaction problem of a gust with a semi-infinite flat plate in a Cartesian system. We use cylindrical polar coordinates $(z_2, \phi_2, x_2)$ for the blades and $(Z_2, Y_2, X_2)$ for the 'unwrapped' system, and both sets of coordinates are locked to the rear row with the $(Z_2, Y_2, X_2)$ coordinate system having its origin at the local blade leading-edge location.

The Cartesian and cylindrical polar systems would normally be linked by the relationships $Z_2 = h_z(z_2 - z_l)$, $Y_2 = h_\phi \phi_2$, $X_2 = h_x x_2$ where $z_l$ is the local dimensionless radius and $h_z = 1$, $h_\phi = z_2$, $h_x = 1$ are the Lamé coefficients. However, for a purely Cartesian system, these coefficients must be constant thus we use $h_\phi = z_l$ where $z_l$ is taken to be constant at the value of the local non-dimensional radius. Thus, for an infinitely small element of the blade leading edge lying between $(z_2, \phi_{LE}(z_2), x_{LE}(z_2))$ and $(z_2 + \mathrm{d}z_2, \phi_{LE}(z_2 + \mathrm{d}z_2), x_{LE}(z_2 + \mathrm{d}z_2))$, where $\phi_{LE} = \phi_{LE}(z_2)$, $x_{LE} = x_{LE}(z_2)$ represent the azimuthal and axial locations of the blade leading edge (see figure 3), the elemental leading edge is given by

$$\mathrm{d}Z_2 = \mathrm{d}z_2, \quad \mathrm{d}Y_{LE} = z_l\,\mathrm{d}\phi_{LE} = z_l \frac{\mathrm{d}\phi_{LE}}{\mathrm{d}z_2}\,\mathrm{d}z_2, \quad \mathrm{d}X_{LE} = \mathrm{d}x_{LE} = \frac{\mathrm{d}x_{LE}}{\mathrm{d}z_2}\,\mathrm{d}z_2. \tag{2.18a–c}$$

In cylindrical blade-fixed coordinates, the leading edge of the rear blade, which varies as a function of $z_2$, lies (relative to its unswept location) at

$$z_2, \quad \phi_{LE}(z_2) = -\frac{\overline{s}_L \sin\alpha_2}{z_2} = -M_t \frac{\overline{s}_L(z_2)}{M_{r_2}(z_2)}, \quad x_{LE}(z_2) = -\overline{s}_L \cos\alpha_2 = -M_x \frac{\overline{s}_L(z_2)}{M_{r_2}(z_2)}, \tag{2.19a–c}$$

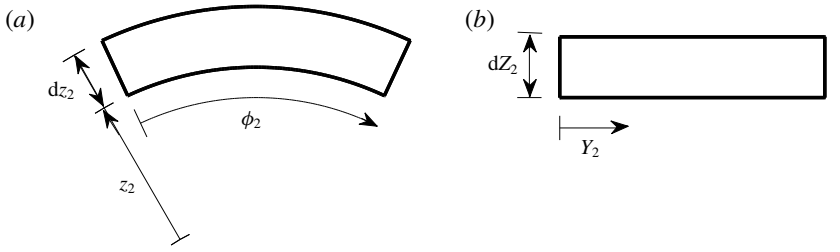


FIGURE 3. Segment of an annulus which lies between $z_2$ and $z_2 + \mathrm{d}z_2$ ($a$). Corresponding unwrapped segment ($b$).

where $\bar{s}_L = 2(s_2 - c_2/2)/D$, so that, combining the axial and azimuthal terms, and using (2.18) and (2.19), we find that elemental changes $\mathrm{d}S_2$ in the non-dimensional sweep in the new Cartesian system – at a fixed radius $Z_2$ – are given by $\mathrm{d}S_2^2 = \mathrm{d}X_{LE}^2 + \mathrm{d}Y_{LE}^2$ or

$$\frac{\mathrm{d}S_2}{\mathrm{d}Z_2} = \sqrt{\left(\frac{\mathrm{d}X_{LE}}{\mathrm{d}Z_2}\right)^2 + \left(\frac{\mathrm{d}Y_{LE}}{\mathrm{d}Z_2}\right)^2} = \sqrt{M_x^2 + z_l^2 M_t^2}\,\frac{\mathrm{d}}{\mathrm{d}z_2}\left(\frac{\bar{s}_L}{M_{r_2}}\right) = M_{r_l}\frac{\mathrm{d}}{\mathrm{d}z_2}\left(\frac{\bar{s}_L}{M_{r_2}}\right). \quad (2.20)$$

The value $\mathrm{d}S_2$ combines the axial and azimuthal movement of the leading-edge location. The value $M_{r_l}$ in (2.20) represents the local relative Mach number in the unwrapped system which is taken to be constant. The net sweep angle of the blade in the unwrapped system is defined as $\Lambda$ with

$$\tan\Lambda = \frac{\mathrm{d}S_2}{\mathrm{d}Z_2} = M_{r_l}\frac{\mathrm{d}}{\mathrm{d}z_2}\left(\frac{\bar{s}_L}{M_{r_2}}\right). \quad (2.21)$$

For reference here we note that an element of leading-edge arc length $\mathbb{s}$ is given by

$$\mathrm{d}\mathbb{s}^2 = \mathrm{d}Z_2^2 + \mathrm{d}S_2^2 = \left\{1 + \left[M_{r_l}\frac{\mathrm{d}}{\mathrm{d}z_2}\left(\frac{\bar{s}_L}{M_{r_2}}\right)\right]^2\right\}\mathrm{d}z_2^2 \quad (2.22)$$

or, equivalently, by $\mathrm{d}\mathbb{s} = \mathrm{d}z_2/\cos\Lambda$ so that the trace velocity of any disturbance along the leading edge of a rear blade is $\sec\Lambda$ times that of the radial disturbance velocity. The swept distance $S_2$ in the Cartesian system can be obtained by integrating (2.21), using $\mathrm{d}Z_2 = \mathrm{d}z_2$, from (2.18), and the fact that $M_{r_l}$ is constant, to get $S_2 = (M_{r_l}/M_{r_2})\bar{s}_L = \bar{s}_L$ at $z_2 = z_l$.

Using the geometry of the original wrapped system, given in § 2, it is easy to show that a wake centreline, lying along Hanson's helicoidal surface and passing through the pitch-change axis of the rear blade, travels a non-dimensional distance $\bar{s}_L(\cos\alpha_2 \tan\alpha_1 + \sin\alpha_2) = z_2(M_{t_1} + M_{t_2})\bar{s}_L/M_{r_2}$ in the negative $\phi_2$ direction to reach the blade leading edge at a non-dimensional speed $z_2(M_{t_1} + M_{t_2})$ relative to the rear blade row. The radial component of the trace Mach number is thus easily obtained as $[\mathrm{d}/\mathrm{d}z_2(\bar{s}_L/M_{r_2})]^{-1}$. In the new unwrapped and untwisted system, the blades are represented by a cascade with non-dimensional leading-edge sweep $S_2$ and sweep angle $\Lambda$. The front and rear blade rows translate in opposite $\phi_2$ directions at Mach numbers $z_l M_{t_1}$ and $z_l M_{t_2}$, respectively, and the relative Mach number of the flow parallel to the rear blade is $M_{r_l}$. A similar geometric analysis shows that the wake

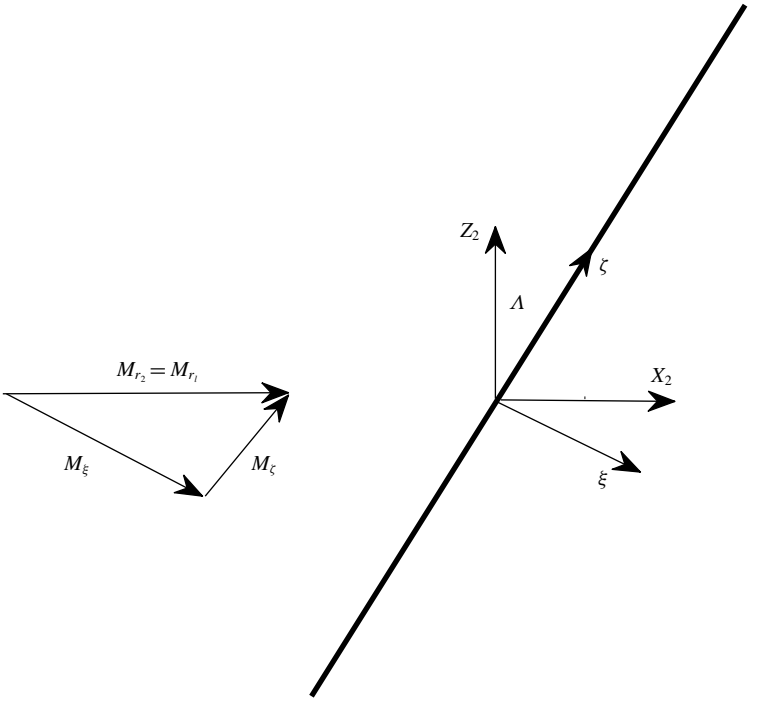


FIGURE 4. Definition of blade leading-edge sweep and local coordinate systems.

centreline travels a non-dimensional distance $z_l(M_{t_1} + M_{t_2})S_2/M_{r_l}$ at a non-dimensional speed $z_l(M_{t_1} + M_{t_2})$ so that the radial component of the trace Mach number along the leading edge of the cascade is obtained as $M_{r_l}/(\mathrm{d}S_2/\mathrm{d}Z_2) = M_{r_l}/\tan\Lambda$ which, from (2.21), is identical to that along the leading edge of the downstream blade row in the original wrapped system.

In order to consider the response of the swept blade in the new unwrapped system, we define new coordinates $(\xi, \chi, \zeta)$ aligned to the local swept blade with

$$X_2 = \xi\cos\Lambda + \zeta\sin\Lambda, \quad Y_2 = \chi, \quad Z_2 = -\xi\sin\Lambda + \zeta\cos\Lambda, \tag{2.23a–c}$$

where $Z_2$ is a normalised radius with its origin centred on the local radial station at which the gust interaction is taking place and $X_2$ is the chordwise or streamwise direction. In this coordinate system, shown in figure 4, each incident harmonic gust defined by (2.14) can then be rewritten as

$$w = w_{n_1}\exp\{\mathrm{i}(k_\xi U_\xi + k_\zeta U_\zeta)\tau - \mathrm{i}k_\xi\xi - \mathrm{i}k_\zeta\zeta - \mathrm{i}k_\chi\chi\}, \tag{2.24}$$

where

$$k_\xi = k_X\cos\Lambda, \quad k_\zeta = k_X\sin\Lambda, \quad k_\chi = k_Y, \quad U_\xi = U_{r_2}\cos\Lambda, \quad U_\zeta = U_{r_2}\sin\Lambda. \tag{2.25a–e}$$

If we assume that, at a local radial station $z$, the swept blade can be considered to be equivalent to a section of an infinite swept aerofoil (as shown in figure 4) with velocities $U_\xi$ and $U_\zeta$ in the $\xi$ and $\zeta$ directions and $(\xi, \chi, \zeta)$ wavenumbers $(k_\xi, k_\chi, k_\zeta)$, then the high-frequency solution to the linearised gust interaction problem in subsonic

compressible flow can be obtained from a Wiener–Hopf analysis, or taken directly from Adamczyk (1974). (The Wiener–Hopf analysis assumes that the aerofoil is semi-infinite in the chordwise direction and represents the interaction of the gust with the leading edge. As we are only interested in predicting the leading-order behaviour of the acoustic field, we apply no correction for the effect of the aerofoil's trailing edge. A discussion of the range of validity of this expression applied to swept thin aerofoils of finite chord length is contained in Adamczyk (1974). For unswept blades Goldstein (1976) states that the total unsteady lift force per unit length calculated using this expression is accurate to within 10% when $M_{r_2}\sigma_2/(1-M_{r_2}^2) > 1$. That expression can be taken to be satisfied here as $\sigma_2$ is directly proportional to $B_1$ and, in line with our high blade number assumption, $B_1 \gg 1$.) Our notation is somewhat different to Adamczyk's, but a little manipulation produces

$$\mathbb{S} = \frac{\mathrm{e}^{-\mathrm{i}\pi/4-\mathrm{i}\sigma_\zeta\overline{\zeta}}}{\pi\sqrt{\pi\overline{\xi}}}\frac{\exp\left[\dfrac{\mathrm{i}\sigma_\xi M_\xi^2 - \mathrm{i}\sqrt{M_\xi^2\sigma_\xi^2-(1-M_\xi^2)\sigma_\zeta^2}}{(1-M_\xi^2)}\overline{\xi}\right]}{\sqrt{\sigma_\xi+\sqrt{M_\xi^2\sigma_\xi^2-(1-M_\xi^2)\sigma_\zeta^2}}}, \tag{2.26}$$

where we have defined the reduced frequencies $\sigma_\xi = k_\xi c_\xi/2$, $\sigma_\zeta = k_\zeta c_\xi/2$, $\overline{\xi}$ and $\overline{\zeta}$ are coordinates normalised by $c_\xi/2$, the normal chord distance is given by $c_\xi = c_2\cos\Lambda$ and our new chordwise coordinate $\overline{\xi}$ has its origin at the leading edge. The dimensional unsteady response is given by $\Delta p_{n_1}(\overline{\xi}) = 2\pi\rho_0 U_{r_2} w_{n_1}\mathbb{S}$ which is consistent with (2.17) but with the dimensional velocity $\sqrt{U_\xi^2+U_\zeta^2} = U_{r_2}$.

After some manipulation, we obtain the unsteady response of the blade to an oblique gust as

$$\mathbb{S}(\sigma_2, M_{r_2}, \Lambda, X_2) = \frac{\mathrm{e}^{-\mathrm{i}\pi/4}\exp\left\{\mathrm{i}\sigma_2\dfrac{\left[(M_{r_2}^2-\tan^2\Lambda)-\sqrt{M_{r_2}^2-\tan^2\Lambda}\right]}{[1-(M_{r_2}^2-\tan^2\Lambda)]}\overline{X}_2\right\}}{\pi\sqrt{\pi\sigma_2\overline{X}_2}\sqrt{1+\sqrt{M_{r_2}^2-\tan^2\Lambda}}}, \tag{2.27}$$

where $\sigma_2 = k_X c_2/2$ and we have switched back to the $(X_2, Y_2, Z_2)$ coordinate system and omitted the terms in $Z_2$, since – for an oblique interaction calculation with a propeller blade at a fixed radius – we must have $Z_2 = 0$. In (2.27) we see that the unsteady response switches from a pure phase variation along the chord to one which is exponentially decaying when $\tan\Lambda > M_{r_2}$. It is interesting to note here, from the definition of the sweep angle in (2.21), that the change occurs at the radius at which $\tan\Lambda = \tan\Lambda^* = M_{r_2}$, in agreement with the solutions of Adamczyk (1974) and Envia & Kerschen (1990) who, along with Graham (1970), discussed the transition point between these super-critical and sub-critical interactions in some detail. (Our solution is simplified relative to Envia & Kerschen's as we have no wake lean, because of the absence of swirl in our case, and no spanwise wake phase angle due to our assumption of quasi-two-dimensional wakes.) Roger *et al.* (2014) and Quaglia *et al.* (2017) presented similar methods for calculating the response of a swept blade to a harmonic gust. It is useful to observe that, in our case, $\tan\Lambda^* = M_{r_2}$ when

$$\frac{\mathrm{d}}{\mathrm{d}z}\left(\frac{\overline{s}_L}{M_{r_2}}\right) = 1. \tag{2.28}$$

By choosing the appropriate branch cut, the solution for $\Lambda > \Lambda^*$ is

$$\mathbb{S}(\sigma_2, M_{r_2}, \Lambda, X_2) = \mathrm{e}^{-\mathrm{i}(\pi/4)+(\mathrm{i}/2)\tan^{-1}\sqrt{\tan^2\Lambda - M_{r_2}^2}} \times \frac{\exp\left\{\sigma_2 \dfrac{\left[-\mathrm{i}(\tan^2\Lambda - M_{r_2}^2) - \sqrt{\tan^2\Lambda - M_{r_2}^2}\right]}{[1+(\tan^2\Lambda - M_{r_2}^2)]}\overline{X}_2\right\}}{\pi\sqrt{\pi\sigma_2\overline{X}_2}[1+(\tan^2\Lambda - M_{r_2}^2)]^{1/4}}, \quad (2.29)$$

where we have incorporated all the phase terms into the exponential argument.

### 2.3. *Acoustic radiation*

Following the derivation presented by Hanson (1985), the far-field tonal sound pressure at 'emission radius' $R_e$, 'emission polar angle' $\theta_e$ (defined such that $\theta_e = 0$ is upstream of the rotor), azimuthal angle $\phi$ and time $t$ (where source time $\tau = t - R_e/c_0$ for a source located at the origin of the coordinate system) produced by the periodic lift forces on the downstream propeller of a contra-rotating open rotor due to the unsteady velocity fields from the upstream propeller can be shown to be given by the following expression

$$p = \frac{\mathrm{i}\rho_0 c_0^2 B_2 D}{8\pi R_e(1 - M_x\cos\theta_e)} \sum_{n_1=-\infty}^{\infty}\sum_{n_2=-\infty}^{\infty} \exp\left\{\mathrm{i}\omega\left(t - \frac{R_e}{c_0}\right) - \mathrm{i}\nu\left(\phi - \frac{\pi}{2}\right)\right\} I_{n_1,n_2}, \quad (2.30)$$

where $I_{n_1,n_2}$ is an integral over non-dimensional radius $z$ from the hub, at $z = z_h$, to the tip at $z = 1$ and which is defined as

$$I_{n_1,n_2} = \int_{z_h}^{1} M_{r_2}^2 \mathrm{e}^{-\mathrm{i}\phi_s} J_\nu\left(\frac{\nu}{z^*}z\right) k_y \frac{C_{Ln_1}}{2}\Psi_{L_{n_1}}(k_x)\,\mathrm{d}z, \quad (2.31)$$

$$\omega = n_1 B_1 \Omega_1 + n_2 B_2 \Omega_2, \quad (2.32)$$

$$\nu = n_2 B_2 - n_1 B_1, \quad (2.33)$$

$$k_x = \frac{2}{M_{r_2}}\left[\frac{(n_1 B_1 M_{T_1} + n_2 B_2 M_{T_2})M_x\cos\theta_e}{(1 - M_x\cos\theta_e)} + \nu M_{T_2}\right]\frac{c_2}{D}, \quad (2.34)$$

$$k_y = -\frac{2}{M_{r_2}}\left[\frac{(n_1 B_1 M_{T_1} + n_2 B_2 M_{T_2})M_{T_2} z\cos\theta_e}{(1 - M_x\cos\theta_e)} - \nu\frac{M_x}{z}\right]\frac{c_2}{D}, \quad (2.35)$$

$$\phi_s = \frac{2}{M_{r_2}}\left[\frac{(n_1 B_1 M_{T_1} + n_2 B_2 M_{T_2})M_x\cos\theta_e}{(1 - M_x\cos\theta_e)} + \nu M_{T_2}\right]\frac{s_2}{D}, \quad (2.36)$$

$$z^* = \frac{(1 - M_x\cos\theta_e)\nu}{(n_1 B_1 M_{T_1} + n_2 B_2 M_{T_2})\sin\theta_e}, \quad (2.37)$$

and the acoustically weighted unsteady lift term at radial station $z$ is given by

$$C_{Ln_1}\Psi_{Ln_1}(k_x) = \int_0^2 \frac{\Delta p_{n_1}(\overline{X}_2)}{\rho_0 U_{r_2}^2}\exp\left\{-\mathrm{i}\frac{k_x}{2}(\overline{X}_2 - 1)\right\}\mathrm{d}\overline{X}_2. \quad (2.38)$$

The value $z^*$ defined by (2.37) is an important parameter, introduced initially as the Mach radius for supersonic straight-bladed single-rotating propellers by Crighton &

Parry (1991); it represents the point at which the argument of the Bessel function in the integrand of (2.31) becomes equal to its order and, significantly, is close to the point at which the Bessel function achieves its maximum value. The behaviour of the Bessel function means that tones for which $n_1$ and $n_2$ are of different signs generally do not radiate efficiently. Also, tones for which $n_1 = 0$ or $n_2 = 0$ occur at the frequencies of the rotor-alone tones produced by each propeller and will not be considered here. Note that each tone consists of contributions from the $\{n_1, n_2\}$ and $\{-n_1, -n_2\}$ terms in the double summation of (2.30). The $\{-n_1, -n_2\}$ term is the conjugate of the $\{n_1, n_2\}$ term and thus we will only consider individual terms from the double summation where $n_1 > 0$ and $n_2 > 0$. When $\Omega_1/\Omega_2$ is a rational number there will be multiple tones occurring at the same frequency, the sum of which would normally be referred to as a single tone. However, in this paper we will refer to the contribution from each $\{n_1, n_2\}$ term in the double summation as a tone.

Having described the full equations for the unsteady response of the downstream blade row to the front propeller wakes, and the resultant sound radiation to the far field, we turn to asymptotic analysis of the formulae. We start by noticing that the Bessel function in (2.31) originates from an integration of the 'noise sources' over a nominal 'source annulus' (see Parry 1988) and we can return to the original, and much more natural, form by replacing it with Bessel's integral

$$J_\nu\left(\frac{\nu}{z^*}z\right) = \frac{1}{2\pi \mathrm{i}^\nu}\int_{-\pi}^{\pi} \exp\left\{\mathrm{i}\nu\left(\frac{z}{z^*}\cos u + u\right)\right\} \mathrm{d}u, \tag{2.39}$$

which allows us to rewrite the noise radiation integral (2.31) in the form

$$I_{n_1,n_2} = \frac{1}{2\pi \mathrm{i}^\nu}\int_{z_h}^{1}\int_{-\pi}^{\pi} G(z)\exp\{\mathrm{i}\nu\Phi(u,z)\}\,\mathrm{d}u\,\mathrm{d}z, \tag{2.40}$$

where $G(z)$ is an amplitude function which incorporates the chordwise Fourier integral of the unsteady lift and is defined as

$$G(z) = \pi M_{r_2} k_y m_{n_1}\int_0^2 \mathbb{S}(\sigma_2, M_{r_2}, \overline{X}_2, \Lambda)\exp\left\{-\mathrm{i}\frac{k_x}{2}\overline{X}_2\right\}\mathrm{d}\overline{X}_2, \tag{2.41}$$

where $m_{n_1} = (\boldsymbol{j}_{Y_2}\cdot\boldsymbol{u}_{n_1})/c_0$. The phase function $\Phi(u,z)$ in (2.40) is defined as

$$\Phi(u,z) = \frac{z}{z^*}\cos u + u - \Gamma(z), \tag{2.42}$$

where $\Gamma(z)$ contains the effects of blade sweep and the effects of the convection of the unsteady velocity field. It is combined from the phase terms of the upwash velocity harmonic in (2.15), from the sweep factor in (2.20) that is defined by (2.36) and from the wavenumber term defined by (2.34) that arises from the integral in (2.38). As we have neglected lean in the current analysis, the mathematical analysis simplifies and we obtain

$$\Gamma(z) = \frac{1}{z^*\sin\theta_e}\frac{\bar{s}_L}{M_{r_2}} + \mathbb{1}\bar{g}\frac{M_{T_1}}{M_x}, \tag{2.43}$$

where $\bar{g} = 2g/D$ and $\mathbb{1} = n_1 B_1/\nu$.

Using the unsteady response function (2.27) in (2.41) we can obtain the acoustically weighted unsteady lift by integrating analytically to produce

$$G(z) = M_{r_2} k_y m_{n_1} \frac{\sqrt{2}\mathrm{e}^{-\mathrm{i}\pi/4}}{\sqrt{\sigma_2 \mathbb{L}_<}\sqrt{1+\sqrt{M_{r_2}^2 - \tan^2\Lambda}}} E\left(2\sqrt{\frac{\mathbb{L}_<}{\pi}}\right), \tag{2.44}$$

where we have defined

$$\mathbb{L}_< = \sigma_2 \frac{\left[(M_{r_2}^2 - \tan^2\Lambda) - \sqrt{M_{r_2}^2 - \tan^2\Lambda}\right]}{[1-(M_{r_2}^2 - \tan^2\Lambda)]} - \frac{1}{2}k_x \tag{2.45}$$

and $E(x) = \mathrm{C}(x) + \mathrm{i}S(x) = \int_0^x \mathrm{e}^{\mathrm{i}(\pi/2)t^2}\mathrm{d}t$ is the complex Fresnel integral (see Gautschi 1970). If $\mathbb{L}_< < 0$ we replace $E(x)$ with $E^*(x) = \mathrm{C}(x) - \mathrm{i}S(x)$ and $\mathbb{L}_<$ with $|\mathbb{L}_<|$ in (2.44). When $\Lambda > \Lambda^*$ and the integrand decays exponentially in the chordwise direction we use the form

$$G(z) = M_{r_2} k_y m_{n_1} \frac{\mathrm{e}^{-\mathrm{i}(\pi/4)+(\mathrm{i}/2)\tan^{-1}\sqrt{\tan^2\Lambda - M_{r_2}^2}}}{\sqrt{\mathbb{L}_>\sigma_2}(1+\tan^2\Lambda - M_{r_2}^2)^{1/4}} \mathrm{erf}(\sqrt{2\mathbb{L}_>}), \tag{2.46}$$

where $\mathrm{erf}(x) = 2/\sqrt{\pi}\int_0^x \mathrm{e}^{-t^2}\,\mathrm{d}t$ is the error function which can be evaluated, for complex arguments, using $\mathrm{erf}(x) = 1 - \mathrm{e}^{-x^2}w(\mathrm{i}x)$ (Gautschi 1970) and we have defined

$$\mathbb{L}_> = \sigma_2 \frac{\sqrt{\tan^2\Lambda - M_{r_2}^2}}{[1+(\tan^2\Lambda - M_{r_2}^2)]} + \mathrm{i}\left\{\frac{(\tan^2\Lambda - M_{r_2}^2)\sigma_2}{[1+(\tan^2\Lambda - M_{r_2}^2)]} + \frac{1}{2}k_x\right\}. \tag{2.47}$$

## 3. Asymptotic evaluation of the radiation integral

As $|\nu|$ becomes large, the integrand of $I_{n_1,n_2}$ defined in (2.40) becomes highly oscillatory due, primarily, to the behaviour of the terms in the argument of the exponential function. This behaviour makes it possible to accurately evaluate the integral using asymptotic methods when $|\nu| \to \infty$.

A number of authors including Jones & Kline (1958), Chako (1965), Bleistein & Handelsman (1969) and Cooke (1982) have considered evaluating double integrals of the form given by (2.40) using asymptotic methods. These studies all demonstrate that the principle contributions to $I_{n_1,n_2}$ arise from small regions of the integrand around certain critical points which for the purposes of the problem considered here can be divided into two general types:

(i) Stationary points of the phase function which occur either within the 'source annulus' or on the bounding curve of the annulus.

(ii) Points on the source annulus boundary where only the tangential derivative of the phase function vanishes.

In the following sections we will present expressions for the leading-order terms in the asymptotic expansion of $I_{n_1,n_2}$. Parry (1995) applied this asymptotic approach to the case of a single-rotating propeller. In that case, however, there was a clear single parameter that could be exploited, namely the number of blades. Here we have two blade rows with different blade numbers (in the general case). We will thus assume

that $\nu$ is a formally large parameter ($|\nu| \to \infty$) and that $B_1 = O(|\nu|)$, $B_2 = O(|\nu|)$ and that linear combinations of $B_1$ and $B_2$ are also $O(|\nu|)$. A natural consequence is that a ratio of these large parameters is $O(1)$. Specifically, we assume that $|z^*| = O(1)$ and $|\mathbb{I}| = O(1)$. These last two assumptions can occasionally be violated in practice for certain tones produced by an open rotor engine, as might be expected.

The asymptotic evaluation of the integral requires the partial derivatives of the phase function which are listed below as

$$\left.\begin{gathered} \Phi_{0,0} = \Phi = \frac{z}{z^*}\cos u + u - \Gamma(z), \\ \Phi_{1,0} = 1 - \frac{z}{z^*}\sin u, \quad \Phi_{0,1} = \frac{\cos u}{z^*} - \Gamma'(z), \\ \Phi_{2,0} = -\frac{z}{z^*}\cos u, \quad \Phi_{1,1} = -\frac{\sin u}{z^*}, \quad \Phi_{0,2} = -\Gamma''(z), \\ \Phi_{3,0} = \frac{z}{z^*}\sin u, \quad \Phi_{2,1} = -\frac{\cos u}{z^*}, \quad \Phi_{1,2} = 0, \quad \Phi_{0,3} = -\Gamma'''(z), \end{gathered}\right\} \tag{3.1}$$

where we have adopted the notation

$$\Phi_{p,q}(u, z) = \frac{\partial^{p+q}}{\partial u^p \partial z^q}\Phi(u, z). \tag{3.2}$$

### 3.1. *Interior stationary points*

We consider first the case of stationary points of the phase function which occur within the source annulus and, adopting the terminology of Chako, will refer to these points as interior stationary points. It is assumed that each of these interior stationary points lie within the source annulus away from the inner and outer edge of the annulus and also separated from other critical points so that the principle contribution to $I_{n_1,n_2}$ from each point can be considered in isolation. (As the interior stationary points approach the boundary, the solutions diverge and uniform asymptotics are needed. There is a discussion of these transition regions in § 6. A similar effect occurs when two (or more) distinct interior stationary points become close to one another.)

An interior stationary point occurs at $\{u, z\} = \{\tilde{u}, \tilde{z}\}$ when $\Phi_{1,0} = \Phi_{0,1} = 0$. For now it will also be assumed that $\Phi_{2,0}\Phi_{0,2} \neq \Phi_{1,1}^2$ at any of these points; when that criterion is not satisfied, the solution is a caustic and it is given in appendix B. From the definition of the partial derivatives we can determine the location of the stationary points to be the solution to the following two equations,

$$\sin\tilde{u} = \frac{z^*}{\tilde{z}}, \quad \cos\tilde{u} = \Gamma'(\tilde{z})z^*, \tag{3.3a,b}$$

or, on eliminating $\tilde{u}$, when

$$\frac{\tilde{z}^2}{z^{*2}} = [\tilde{z}\Gamma'(\tilde{z})]^2 + 1. \tag{3.4}$$

Equation (3.4) is one of the main results of the paper as, in the general case, it defines the radial locations on the rear blade from which the peak noise is radiated. In applying asymptotic analysis to the radiation integral we are exploiting the fact

that the phase variations across the propeller source annulus, are such that the acoustic radiation is largely self-cancelling – apart from those small regions where the phase becomes stationary. The far-field sound is thus completely dominated by that generated at the locations that are given (in terms of non-dimensional radii) by the solutions to (3.4), and, furthermore, the azimuthal locations can also be determined from the solution to (3.3). The resultant acoustic radiation is then given by the algebraic solutions (3.7) and (3.8), below, where the source amplitudes are taken solely from the locations defined by (3.4). It might be expected that the result (3.4) is, on its own, insufficient to determine the radial locations that dominate the sound field as a key factor, when the rear blade is swept, is the trace velocity of the wake along the blade leading edge and, in particular, the radial station at which the gust transitions from super-critical to sub-critical. However, we show in § 4.1, below, that both criteria are completely consistent and that (3.4) alone is sufficient. It is also possible to consider cases in which the solution to (3.4) represents not just a single radial station $\tilde{z}$ but a continuous distribution $\tilde{z}(z)$ of stationary phase points across the propeller source annulus. Such cases – or critical designs – are considered below in § 4.2. It should be added that the radial locations $\tilde{z}$, given by (3.4), are functions of the far-field radiation angle $\theta_e$ because $\tilde{z}$ is dependent on the Mach radius $z^*$ and, from (2.37), $z^* = z^*(\theta_e)$. Thus – as might be expected – the location of the stationary phase points on the propeller source annulus $[\tilde{z}(\theta_e), \tilde{u}(\theta_e)]$, that dominate the acoustic radiation, vary with far-field radiation direction. These points can thus enter or leave the domain as the far-field observer moves in a polar arc around the propeller which, as we might expect, can result in strong variations in the far-field directivity – as we will show in § 6 below.

We follow the method of Cooke (1982) to evaluate the contribution to $I_{n_1,n_2}$ from an interior stationary point for $|\nu| \to \infty$. Expanding $G$ in a Taylor series about $z = \tilde{z}$ and $\Phi$ in a double Taylor series about $z = \tilde{z}$, $u = \tilde{u}$ we obtain the leading-order contribution from the stationary point as

$$I_{n_1,n_2} \sim \frac{\tilde{G}}{2\pi \mathrm{i}^{\nu}} \exp\{\mathrm{i}\nu\tilde{\Phi}_{0,0}\} \int_{-\infty}^{\infty}\int_{-\infty}^{\infty} \exp\left\{\mathrm{i}\frac{\nu}{2}\left[\left(\tilde{\Phi}_{0,2} - \frac{\tilde{\Phi}_{1,1}^2}{\tilde{\Phi}_{2,0}}\right)Z^2 + \tilde{\Phi}_{2,0}U^2\right]\right\} \mathrm{d}U\,\mathrm{d}Z, \tag{3.5}$$

where the tilde over a parameter indicates that it is evaluated at the stationary point $z = \tilde{z}$, $u = \tilde{u}$ and we have used the simple transform

$$Z = z - \tilde{z}, \quad U = (u - \tilde{u}) + \frac{\tilde{\Phi}_{1,1}}{\tilde{\Phi}_{2,0}}(z - \tilde{z}), \tag{3.6a,b}$$

for which the Jacobian is unity. The double integral is easily evaluated as

$$I_{n_1,n_2} \sim \frac{\tilde{G}}{|\nu|\sqrt{|\tilde{\Phi}_{2,0}\tilde{\Phi}_{0,2} - \tilde{\Phi}_{1,1}^2|}} \exp\left\{\mathrm{i}\nu\left(\tilde{\Phi}_{0,0} - \frac{\pi}{2}\right) + \mathrm{i}\frac{\pi}{4}\mathrm{sgn}(\nu)\mathrm{sgn}(\tilde{\Phi}_{2,0})[1 + \mathrm{sgn}(\tilde{\Phi}_{2,0}\tilde{\Phi}_{0,2} - \tilde{\Phi}_{1,1}^2)]\right\}. \tag{3.7}$$

For the case when an interior stationary point lies at the edge of the annulus i.e. $\tilde{z} = z_h$ or $\tilde{z} = 1$ then the range of integration over $Z$ in (3.5) should be either $0 < Z < \infty$ (for $\tilde{z} = z_h$) or $-\infty < Z < 0$ (for $\tilde{z} = 1$). This yields a result for the leading-order term which is equal to half that given by (3.7).

We have thus obtained a simple algebraic result that retains the physics of the full numerical solution, yet it contains no integration and no special functions and merely requires the evaluation of the amplitude function $G(z)$ at the critical radius $z=\tilde{z}$ and the partial derivatives $\Phi_{p,q}$ at $z=\tilde{z}$, $u=\tilde{u}$. In addition, we have found that the leading-order asymptotic solution is $O(|\nu|^{-1})$.

Cases for which $\Gamma'(z)=0$ are not given directly by (3.7) as, in that case, we have $\tilde{\Phi}_{0,2}=0$ and since, from (3.1), $\cos\tilde{u}=0$ we also have $\tilde{\Phi}_{2,0}=0$. The solution for these cases is given by

$$I_{n_1,n_2} \sim \frac{\tilde{G}|z^*|}{|\nu|}\exp\left\{\mathrm{i}\nu\left(\tilde{\Phi}_{0,0}-\frac{\pi}{2}\right)\right\}, \tag{3.8}$$

where we have put $|\tilde{\Phi}_{1,1}|=1/|z^*|$ and used the transformation $u-\tilde{u}=(Z+U)/2$ and $z-\tilde{z}=(Z-U)/2$ for which the Jacobian is $1/2$. This result, like (3.7), is of $O(|\nu|^{-1})$.

For completeness, we also note that the on-axis results ($\theta_e=0$ or $\pi$) are not given by (3.7). In those cases the phase function (2.42) reduces to $\Phi(u,z)=u-\Gamma(z)$ so that the double integral (2.40) can be split directly and the trivial evaluation of the $u$-integral produces $I_{n_1,n_2}=0$. Of course, close to the axis in the range for which $\theta_e=O(|\nu|^{-1})$, a separate approach would be needed as the term $z/z^*\cos u$ in the phase function (2.42) would also be $O(|\nu|^{-1})$.

It is important to emphasise that the accuracy of the solution depends not just on the fundamentals of the asymptotic approach, but also on the validity of the models for the unsteady velocity fields and the blade response. To both understand the accuracy, and demonstrate the power, of the asymptotic approach we will compare the asymptotic solutions with numerical results in § 6.

We extend our analysis to consider the contribution to the radiated sound field from interior stationary points of higher order in appendix B.

### 3.2. *Boundary critical points*

If no stationary points exist within the domain of integration then the main contributions to $I_{n_1,n_2}$ come from what we will refer to as boundary critical points. Boundary critical points are those points on the boundary of the domain of integration at which only the tangential derivative of $\Phi$ vanishes. Therefore, the tangential derivative of $\Phi$ vanishes on the boundary when $\Phi_{1,0}=0$ and $z=z_t=1$ or $z=z_h$. From (3.1), the boundary critical points arise at $\sin u=z^*/z_{t,h}$ producing two solutions at both the tip and the hub, $z=\hat{z}=z_{t,h}$, $u=\hat{u}_\pm$, where

$$\hat{u}_\pm=\begin{cases}\sin^{-1}(z^*/z_{t,h})\\ \pi\mathrm{sgn}(z^*)-\sin^{-1}(z^*/z_{t,h}),\end{cases} \tag{3.9}$$

in which $\hat{u}_+$ and $\hat{u}_-$ are defined by the upper and lower expressions to the right of the curly brace, respectively. When there are no stationary points on the propeller source annulus, the rapid phase variation ensures that the acoustic radiation is almost completely self-cancelling – apart from at those critical points on the boundary. The boundary radial locations are clearly the tip and hub and the azimuthal locations are given by the solution to (3.9). Whilst the radial locations are fixed, the azimuthal locations are functions of the far-field radiation angle $\theta_e$ as, in (3.9), $z^*=z^*(\theta_e)$. Since we must have $|\sin\hat{u}_\pm(\theta_e)|\leqslant 1$ it is thus possible for hub or tip boundary points to appear or disappear as the observer location varies. Such events will impact on the

far-field directivity – as will be shown in § 6. The resultant algebraic solutions for the boundary critical points are given by (3.12) below.

When $|z^*| > 1$ there is no solution for $\hat{u}_\pm$. In this case, the tones do not have critical points either on the boundary or within the interior of the annulus and, as a result, do not radiate efficiently to the far field. Their behaviour can be understood by considering the behaviour of the Bessel function in the integrand of the original formulation, equation (2.31), in which, when $|z^*| > 1$ and $|\nu| \to \infty$ the Bessel function may be replaced by its large-order asymptotic form

$$J_\nu\left(\nu\frac{z}{z^*}\right) \sim \frac{\exp\{|\nu|(\tanh(\alpha)-\alpha)\}}{\sqrt{2\pi|\nu|\tanh(\alpha)}}, \tag{3.10}$$

where $\mathrm{sech}(\alpha) = z/z^*$, $\alpha > 0$. This expression decays exponentially with $|\nu|$ for all possible values of $z$ when $|z^*| > 1$ and thus the resultant far-field sound pressure level for these tones will be low. (We note, in passing, that the approximation in (3.10) was used by Parry & Crighton (1989*b*) to explore the tones from a subsonic single-rotating propeller and their far-field behaviour.) The exponential decay reflects the fact that, for these tones and directions, the sound field is completely self-cancelling. Experimental evidence confirming such behaviour has been presented in Kingan *et al.* (2014) where it was observed that only interaction tones for which $|z^*| < 1$ were observed in the far-field noise spectrum produced by a model-scale advanced open rotor.

Following the method presented in Cooke (1982) we find that the two contributions $I^{\pm}_{n_1,n_2}$ from the tip to $I_{n_1,n_2}$ are, to leading order, given by

$$I^{\pm}_{n_1,n_2} \sim \frac{\hat{G}\exp\{\mathrm{i}\nu\hat{\Phi}_{0,0}\}}{2\pi\mathrm{i}^\nu}\int_{-\infty}^{1}\exp\{\mathrm{i}\nu\hat{\Phi}_{0,1}(z-1)\}\,\mathrm{d}z\int_{-\infty}^{\infty}\exp\left\{\mathrm{i}\frac{\nu}{2}\hat{\Phi}_{2,0}(u-\hat{u}_\pm)^2\right\}\mathrm{d}u, \tag{3.11}$$

where the hat on a parameter indicates that it is evaluated at $z = \hat{z}$, $u = \hat{u}_\pm$. The integrals are easily calculated as

$$I^{\pm}_{n_1,n_2} \sim \frac{\hat{G}\exp\left\{\mathrm{i}\nu\hat{\Phi}_{0,0} + \mathrm{i}\frac{\pi}{4}\mathrm{sgn}(\nu)\mathrm{sgn}(\hat{\Phi}_{2,0})\right\}}{\mathrm{i}^{\nu+1}\sqrt{2\pi}\nu|\nu|^{1/2}|\hat{\Phi}_{2,0}|^{1/2}\hat{\Phi}_{0,1}}. \tag{3.12}$$

For the hub, the only difference is that the integral over $z$ in (3.11) runs from $z = z_h$ to $z = \infty$ so that the result is the negative of (3.12) and with the hat on a parameter indicating that it is to be evaluated at $z = \hat{z} = z_h$. Note that if $|z^*| > z_h$ there will be no critical point on the boundary at the hub (and therefore contributions from the hub region can be neglected).

This result (3.12) becomes singular, and invalid, when either $\hat{\Phi}_{0,1} = 0$, which represents the case in which the boundary critical point is actually an interior stationary phase point located at the tip or hub, or when $\hat{\Phi}_{2,0} = 0$ which, from (3.1), represents either an observer direction corresponding to an infinite Mach radius $|z^*|$, which occurs on axis, or at an observer direction corresponding to a Mach radius equal to the tip or hub so that $|z^*| = z_{t,h}$. As we have already explained, the Mach radius located at the tip represents the limit of a radiating solution; for either hub or tip case, however, it is easy to use (2.37) and (3.1) to determine the corresponding observer direction $\theta_e$. As we will show below, it is important to exclude the solution at and close to these observer directions.

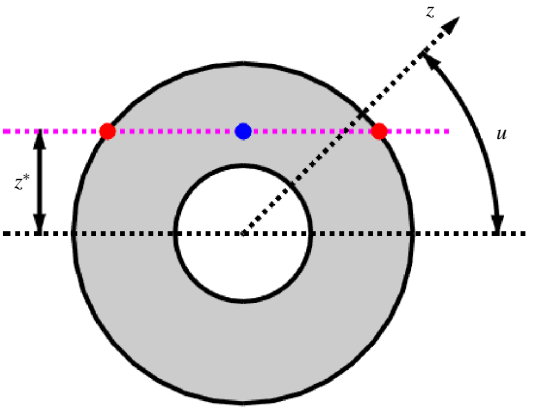


FIGURE 5. (Colour online) The propeller source annulus. An interior stationary point and two boundary critical points are shown as solid circles.

Once again, we have obtained simple algebraic formulae that, nonetheless, describe the behaviour of the contributions to the radiation integral from the hub and tip. In (3.12) we have shown that the contributions from the boundary critical points are $O(|\nu|^{-3/2})$, compared to the $O(|\nu|^{-1})$ solution obtained for an interior stationary point. We would thus expect the radiated sound level from boundary critical point tones to be relatively lower.

Figure 5 shows the location of an interior stationary point and two boundary critical points on the source annulus for a particular tone. From (3.3) and (3.9) it is clear that all critical points are located a distance $z^*$ from the $u=0$ axis.

## 4. Asymptotics and blade sweep

It is now important to assess the implications of the asymptotic analysis on blade sweep and we consider two important points. Firstly, how do we reconcile the key interior stationary point solution (3.4) with the well-known unsteady aerodynamic solutions for sub and supercritical gusts? Secondly, is blade sweep always beneficial (or neutral) for noise or can it lead to enhancement of the sound field?

### 4.1. *Blade sweep and interior stationary point locations*

Recall, from (3.4), that for $|z^*|>0$, interior stationary points (if they occur) are located at radii $\tilde{z}$ which satisfy $\tilde{z}^2/z^{*2}=[\tilde{z}\Gamma'(\tilde{z})]^2+1$. Therefore, from (2.43) and (3.4), interior stationary points satisfy

$$\frac{\tilde{z}^2}{z^{*2}}=1\Bigg/\left\{1-\left[\frac{1}{\sin\theta_e}\frac{\mathrm{d}}{\mathrm{d}z}\left(\frac{\bar{s}_L}{M_{r_2}}\right)\right]^2\right\}. \tag{4.1}$$

In § 2.2 it was shown that the local leading-edge sweep could be described in terms of a local leading-edge sweep angle $\Lambda$ which combines both the axial and the tangential components of blade sweep and is related to $\bar{s}_L$ by $\tan\Lambda=M_{r_2}\mathrm{d}/\mathrm{d}z(\bar{s}_L/M_{r_2})$ so that (4.1) becomes

$$\frac{\tilde{z}}{z^*}=1\Bigg/\sqrt{1-\left[\frac{\tan\Lambda}{M_{r_2}\sin\theta_e}\right]^2}. \tag{4.2}$$

Here, of course, both $\Lambda$ and $M_{r_2}$ are functions of $\tilde{z}$ so that (4.2) represents a nonlinear equation in $\tilde{z}$. Equivalently, using the discussion in § 3.1, we could express the azimuthal location of the interior stationary point as

$$\sin\tilde{u} = \sqrt{1 - \left[\frac{\tan\Lambda}{M_{r_2}\sin\theta_e}\right]^2} \tag{4.3}$$

so that, from (4.2) and (4.3), it is clear that there are no solutions for $\tilde{z}$ if $\tan\Lambda > M_{r_2}$. In § 2.2 we showed that the chordwise variation in the response switches from an oscillatory phase variation to one which is exponentially decaying at precisely this point: $\Lambda = \Lambda^* = \tan^{-1}(M_{r_2})$. The result is well known (see Graham (1970) and the detailed discussions in Adamczyk (1974) and Envia & Kerschen (1990)) and is generally described as the change from a super-critical to a sub-critical gust response. However, in appendix A we show that the amplitude of the acoustically weighted response integrated over the chord remains of the same order of magnitude whether the interaction is super- or sub-critical. Since the acoustically weighted response determines the magnitude of the radial amplitude function $G(z)$ defined in (2.41) and, thereby, the value of $\tilde{G}$ used in the final interior stationary point solution (3.8), we might have expected the switch between super- and sub-critical regions to have no bearing on the locations of the interior stationary points, particularly as it has little bearing on the magnitude of $G(z)$. Furthermore, the unsteady aerodynamic response is produced at a fixed frequency, $n_1B_1(\Omega_1 + \Omega_2)$, and is independent of the direction in which sound is radiated whilst the interior stationary point locations depend on the scattered frequency, $n_1B_1\Omega_1 + n_2B_2\Omega_2$, and on the radiation direction $\theta_e$. Nonetheless, the results (4.2) and (4.3) show that sweeping the downstream blade to produce locally sub-critical gusts affects both the blade response and the radial locations that dominate acoustic radiation.

Moreover, we can qualify the effect of a sub-critical gust on the radiation directivity from an interior stationary point. From (4.2), as $\tan\Lambda$ increases, with $\tan\Lambda < M_{r_2}$, the region of sound radiation, where it is possible for an interior critical point to exist, reduces as $\Lambda$ approaches $\tan^{-1}(M_{r_2})$. Since the term in braces in (4.2) must be positive for a solution to exist we find that the region of radiation is governed by

$$\sin^{-1}\left(\frac{\tan\Lambda}{M_{r_2}}\right) \leqslant \theta_e \leqslant \pi - \sin^{-1}\left(\frac{\tan\Lambda}{M_{r_2}}\right), \tag{4.4}$$

so that the radiation becomes restricted to a narrow region close to the nominal propeller plane.

Despite the fact that the switch from a super- to a sub-critical interaction affects the unsteady gust response for a swept blade, it remains the case that the sound radiation is governed by the interior stationary point solutions (if they exist) to (3.4). We will thus analyse this expression in more detail.

### 4.2. *Critical blade designs*

We consider a case in which (3.4), which defines the radial locations that dominate the sound field, is valid not just at a single radial station but across all radii between the hub and the tip. It will be convenient to introduce the parameter $\Theta(z) = \bar{s}_L/M_{r_2}\sin\theta_e$ so that

$$\Gamma'(z) = \frac{1}{z^*}\Theta'(z). \tag{4.5}$$

Substituting (4.5) into (3.4) and rearranging yields

$$\Theta_c'(z) = \sqrt{1 - \left(\frac{z^*}{z}\right)^2}, \quad z \geqslant |z^*|, \tag{4.6}$$

which defines a 'critical blade design' for which there is a continuum of interior stationary points on the source annulus. Blade designs for which $\Theta'(z)$ is larger than that defined by (4.6) at all radii will have no interior stationary points located within the source annulus.

Integrating (4.6) gives

$$\Theta_c(z) = |z^*|\left\{\sqrt{\frac{z^2}{z^{*2}} - 1} - \tan^{-1}\sqrt{\frac{z^2}{z^{*2}} - 1}\right\} + C, \quad z \geqslant |z^*|, \tag{4.7}$$

where $C$ is an arbitrary constant.

The 'critical sweep' that produces a critical blade design is therefore given by

$$\bar{s}_L(z) = M_{r_2} \sin\theta_e \Theta_c(z), \quad z \geqslant |z^*|, \tag{4.8}$$

which shows that the form of the critical design is, functionally, very similar to that obtained by Parry (1995) for the rotor-alone tone of a single-rotating propeller. For this design, the noise radiation is dominated not just by that from a specific radius but from a continuum of points spread along a line between the hub and the tip.

In order to consider the noise radiated by this critical design we now return to the definition of the phase term $\Phi$ in the radiation integral. Since the two arguments $u$ and $z$ represent azimuthal and radial locations on the source annulus, we consider a change of coordinates to

$$X = z\cos u, \quad Y = z\sin u, \tag{4.9a,b}$$

by which, after differentiating with respect to $X$ and $Y$, we find that $\Phi$ has stationary points at

$$Y = z^*, \quad 0 < X < \sqrt{1 - z^{*2}}, \tag{4.10a,b}$$

showing that the interior stationary point solutions lie as a continuum along one half of the plane defined by $Y = z^*$.

The radiation integral (2.40) can now be evaluated asymptotically in a manner similar to that used for single-rotating propellers Parry (1995) and we simply quote the result as

$$I_{n_1,n_2} \sim \sqrt{\frac{|z^*|}{2\pi|\nu|}}\exp\left\{\mathrm{i}\nu D - \mathrm{i}\frac{\pi}{4}\right\}\int_{|z^*|}^{1}\frac{G(z)}{(z^2 - z^{*2})^{1/4}}\,\mathrm{d}z. \tag{4.11}$$

For the case where $|z^*| < z_h$, we obtain an identical expression to (4.11) but with the lower limit of integration set to $z_h$.

As before, we have obtained an expression which retains the complete physics of the full solution but which is significantly reduced in complexity; however, in this case, the solution does contain a radial integral with the integrand in (4.11) representing a modulation of the amplitude function $G(z)$ such that the integrand becomes weakly

singular at the sonic radius so that the contribution from this region is enhanced. The presence of an integral here is to be expected as it represents a summation of the contributions from a continuum of interior stationary points between the hub and the tip. It is of particular importance to note that the result (4.11) is $O(|\nu|^{-1/2})$ and is thus of higher order than that from boundary critical points which are $O(|\nu|^{-3/2})$, interior stationary points which are $O(|\nu|^{-1})$, and even caustic solutions (described in appendix B), which are $O(|\nu|^{-5/6})$. All straight-bladed propellers have (at most) a single interior stationary point with radiation of $O(|\nu|^{-1})$. The design defined by (4.7) and (4.8) thus produces increased radiation relative to a straight-bladed propeller showing that sweep is not necessarily beneficial.

In appendix C we show the results for a simple case in which the amplitude function $G(z)$ is taken to be approximately constant, with $G(z) = G_0$. The result (4.11) can then be evaluated directly in terms of elliptic integrals.

## 5. Asymptotics – special cases

For cases in which the values of $n_1$ and $n_2$ produce a mode order $\nu$ that cannot be considered large, we cannot use the results of §§ 3 and 4 directly. Instead, we suppose that $|\nu| = O(1)$ and, as the blade numbers $B_1$ and $B_2$ are both still large, let $\eta \to \infty$ where $\eta = n_1 B_1 M_{T_1} + n_2 B_2 M_{T_2}$. The special case in which $\nu = 0$ (and thus $z^* = 0$) is discussed partly in § 5.2 and in more detail in appendix D.

### 5.1. *Special case:* $\nu = O(1)$

In the asymptotic analysis for the many-bladed propeller presented above we have assumed that $|\nu| \to \infty$ is our formally large parameter with $B_1 = O(|\nu|)$, $B_2 = O(|\nu|)$. However, there are instances in which certain combinations of $n_1$ and $n_2$ produce $|\nu| = O(1)$, even though $B_1$ and $B_2$ are still large. In order to analyse such tones we define a formally large parameter $\eta = n_1 B_1 M_{T_1} + n_2 B_2 M_{T_2}$ with $\eta \to \infty$ and rewrite the radiation integral (2.31) as

$$I_{n_1,n_2} = \frac{1}{2\pi \mathrm{i}^{\nu}} \int_{z_h}^{1} \int_{-\pi}^{\pi} G(z) \exp\{\mathrm{i}\eta \Phi^{\dagger}(u, z)\} \, \mathrm{d}u \, \mathrm{d}z, \tag{5.1}$$

where $\Phi^{\dagger}(u, z)$ is a phase function, defined as

$$\Phi^{\dagger}(u, z) = \frac{z}{z^{\dagger}} \cos u + \varepsilon u - \Gamma^{\dagger}(z), \tag{5.2}$$

with $\varepsilon = \nu/\eta \ll 1$,

$$\Gamma^{\dagger}(z) = \frac{1}{(1 - M_x \cos\theta_e)} \frac{\bar{s}_L}{M_{r_2}} + \Lambda^{\dagger} \bar{g} \frac{M_{T_1}}{M_x}, \tag{5.3}$$

$z^{\dagger} = (1 - M_x \cos\theta_e)/\sin\theta_e$ and $\Lambda^{\dagger} = n_1 B_1/\eta = O(1)$. As in § 3, the phase variation around the propeller source annulus varies rapidly with non-dimensional radius $z$ and azimuthal angle $u$ due to the large value of $\eta$ in (5.1). The radiation will thus be dominated by those points at which the phase function $\Phi^{\dagger}$ becomes stationary. The required first-order derivatives of (5.2) are

$$\Phi^{\dagger}_{1,0}(u, z) = \varepsilon - \frac{z}{z^{\dagger}} \sin u, \quad \Phi^{\dagger}_{0,1}(u, z) = \frac{1}{z^{\dagger}} \cos u - \Gamma^{\dagger\prime}(z), \tag{5.4a,b}$$

so that interior stationary points occur when $z\sin u = \varepsilon z^\dagger = z^*$, $\cos u = z^\dagger \Gamma^{\dagger\prime}(z) = z^* \Gamma'(z)$ i.e. the interior stationary points, that represent the regions that dominate sound radiation, occur at the same locations on the source annulus as the $|\nu| \to \infty$ solutions.

In order to better understand the solution in this case we consider, first, a straight-bladed propeller (that is with a straight leading edge i.e. $\bar{s}_L = 0$) such that $\Gamma^{\dagger\prime}(z) \equiv 0$. We find that interior stationary points occur when $u = \mathrm{sgn}(\varepsilon)\pi/2 = \mathrm{sgn}(z^*)\pi/2$ and $\tilde{z} = |\varepsilon| z^\dagger = |z^*|$, provided $z_h \leqslant \tilde{z} \leqslant 1$. The result is identical to that of § 3.1 except that, for these $|\nu| = O(1)$ cases, the interior stationary point lies a distance $\varepsilon z^\dagger = z^*$ from the $u = 0$ plane (see figure 5) and this distance is small provided $|\varepsilon| z^\dagger = |z^*| \ll 1$. Since $\varepsilon \ll 1$ it is thus clear that, in the general case with $z^\dagger = O(1)$, any stationary points of $\Phi^\dagger$ will almost certainly lie inside the hub and, therefore, outside of the source annulus. Interior stationary points, which are shown to produce sound radiation of $O(\eta^{-1})$, can exist but will only occur at angles close to the flight axis where $\varepsilon z^\dagger = O(1)$. Precisely, interior stationary points can only occur in the forward arc at observer angles for which $\theta_e \leqslant (1 - M_x)|\varepsilon|/z_h$. For polar angles greater than this, the leading-order contribution to the sound field will come from boundary critical points on the hub and tip which are of lower order in $\eta$. For high-frequency tones with low azimuthal mode order we have thus found via asymptotic analysis that the solution will be dominated by radiation close to the flight axis. However, provided $\varepsilon \neq 0$, there is a lower limit on $\theta_e$, set by the blade tip, and the interior stationary points will move out of the propeller source annulus again as $\theta_e$ reduces still further: precisely, the radiation will be dominated by the region $(1 - M_x)|\varepsilon| < \theta_e < (1 - M_x)|\varepsilon|/z_h$ in the forward arc (a similar analysis can be done in the rear arc). An example of this effect can be seen in figure 6 in § 6.1 for which the interior stationary points only occur close to the propeller axis and where the solution is clearly dominated by the near-axis results but with the solution still reducing rapidly as the axis is approached.

For the general case with $\Gamma^{\dagger\prime}(z) \neq 0$, the azimuthal locations of interior stationary points are not given by $u = \mathrm{sgn}(\varepsilon)\pi/2$ but by (5.4) which is governed by the value of $\Gamma^{\dagger\prime}(z)$ thus allowing interior stationary points to occur for any observer location $\theta_e$ provided the sweep is sufficient. At the very least, sweep modifies the angular region over which stationary points occur (increasing both the upper and lower limits of the range of polar angles where interior stationary points occur). For $\theta_e \ll 1$, we can demonstrate the change in the angular range by proceeding as above whence we find that interior stationary point solutions will occur at angles for which $\theta_e \approx (1 - M_x)\sqrt{[\Gamma^{\dagger\prime}(z)]^2 + (|\varepsilon|/z)^2}$, where $z_h \leqslant z \leqslant 1$. Consequently, we have discovered that, for these tones with low azimuthal mode order $[|\nu| = O(1)]$ and high frequency $(\eta \to \infty)$, the effect of sweep is likely to increase the interaction noise compared to a straight-bladed rear propeller, in regions away from the flight axis, as interior stationary points are introduced into the solution. These effects can be observed in the comparisons in §§ 6.1 and 6.2; see, particularly, figures 6 and 9 for the $n_1 = 2$, $n_3 = 3$ interaction and the accompanying discussion.

Following the procedure described above it is straightforward to show that the leading-order asymptotic expressions for interior stationary and boundary critical points are identical to those obtained in §§ 3.1 and 3.2. Written in terms of the asymptotic approach described in this section, these solutions are $O(\eta^{-1})$ for interior stationary points and $O(\eta^{-3/2})$ for boundary critical points. Also, as might be expected, an identical expression for the critical blade sweep design to that obtained in § 4.2 is obtained which produces $O(\eta^{-1/2})$ solutions. As in § 4.1, this critical blade design has a continuum of stationary phase points – that dominate the acoustic radiation – distributed between hub and tip. For $\varepsilon \ll 1$, however, we can integrate the expression

$[z^\dagger \Gamma^{\dagger\prime}(z)]^2 = 1 - [\varepsilon z^\dagger/z]^2$ and obtain a simplified expression for the critical blade design as

$$\bar{s}_L \sim (z - z_h)\left[1 - \frac{1}{2}\frac{(\varepsilon z^\dagger)^2}{z z_h}\right] M_{r_2} \sin\theta_e, \tag{5.5}$$

where we have arranged the integration constant so that the leading edge sweep is zero at the hub. Of course, the same result could be obtained by using $z^* = \varepsilon z^\dagger$ in (4.7), expanding for $\varepsilon \ll 1$, and using the result in (4.8).

### 5.2. *Special case:* $\nu = 0$

In appendix D it is shown that when $\nu = 0$, the radiation integral defined by (2.40) can be evaluated using asymptotic methods for $\eta \to \infty$ as the phase in the radiation integral still varies rapidly so that the result is dominated by regions on the propeller source annulus at which the phase becomes stationary or at points on the boundary (tip or hub) at which the contributions are not self-cancelling. In these cases, $|z^*| = 0$, so that the Mach radius lies on the propeller axis and the circumferential phase speed of the $\{n_1, n_2\}$ tone is supersonic at all radii between hub and tip, and interior stationary points occur when $u = 0$, $\pi$ and $\Gamma^{\dagger\prime}(z) = \pm 1/z^\dagger$, respectively, where $\Gamma^\dagger$ and $z^\dagger$ are defined in § 5.1 and $z^\dagger$ is independent of $z$. A critical design, with stationary phase points that dominate the radiation spread between hub and tip, satisfies $\Gamma^\dagger(z) = (z - z_h)/z^\dagger + \Lambda^\dagger \bar{g} M_{T_1}/M_x$ so that, from (5.3), we obtain the critical blade leading-edge sweep as

$$\bar{s}_L(z) = (z - z_h) M_{r_2} \sin\theta_e, \tag{5.6}$$

in which the sweep varies purely linearly with radius. This result can also be obtained either by letting $\varepsilon \to 0$ in § 5.1 or by letting $z^* \to 0$ in (4.7) and then inserting the result into (4.8).

Of perhaps more interest here is a discussion of the physics associated with the solution along the rotor axis. When $\nu = 0$ and $\theta_e = 0$ or $\pi$, the acoustic radiation integral (5.1) reduces to

$$I_{n_1,n_2} = \int_{z_h}^{1} G(z) \exp\{-\mathrm{i}\eta \Gamma^\dagger(z)\}\, \mathrm{d}z. \tag{5.7}$$

Since this integral is only over $z$ it can be evaluated, for large $\eta$, by the one-dimensional stationary phase method as

$$I_{n_1,n_2} \sim G(\tilde{z}) \sqrt{\frac{2\pi}{\eta |\Gamma^{\dagger\prime\prime}(\tilde{z})|}} \exp\left\{-\mathrm{i}\eta \Gamma^\dagger(\tilde{z}) - \mathrm{i}\frac{\pi}{4}\mathrm{sgn}[\Gamma^{\dagger\prime\prime}(\tilde{z})]\right\}, \tag{5.8}$$

where $z = \tilde{z}$ is the radial station at which the phase becomes stationary, or $\Gamma^{\dagger\prime}(\tilde{z}) = 0$. The solution is $O(\eta^{-1/2})$ and is thus of the same order as that from a design with critical sweep for which the radiation arises from a radial continuum of points. The result can be interpreted as a circumferential ring, or continuum, of stationary points at $z = \tilde{z}$ which focus their radiation along the axis. If there are no stationary points the solution to (5.8) comes solely from the endpoints at $z = z_h$ and $z = 1$ and we find that the leading-order contributions are

$$I_{n_1,n_2} \sim \left[\frac{\mathrm{i} G(z) \exp[-\mathrm{i}\eta \Gamma^\dagger(z)]}{\eta \Gamma^{\dagger\prime}(z)}\right]_{z=z_h}^{z=1}, \tag{5.9}$$

which also represents circumferential rings of sources at the hub and tip. The result (5.9) is $O(\eta^{-1})$ and, although it is an endpoint or boundary contribution, it is interesting to note that it is of the same order as the regular interior stationary point solution obtained in § 3.1.

Of even greater interest is the case of a straight-bladed propeller for which we have $\Gamma^{\dagger}(z)$ equal to a constant. For such a configuration, the radiation along the axis reduces to the simple integral

$$I_{n_1,n_2} = \exp\{-\mathrm{i}\eta\Gamma^{\dagger}\}\int_{z_h}^{1} G(z)\,\mathrm{d}z. \tag{5.10}$$

This is an important result and shows that the radiation along the axis for a zero-order circumferential mode ($\nu = 0$) produced by a straight-bladed propeller is $O(1)$. We would, therefore, expect the radiated sound levels on axis to be significantly higher than that from critical designs, caustics or interior stationary points at any point in the radiated sound field. Since all radial and circumferential point contributions are of equal magnitude, and as (5.10) is $O(1)$ – higher by $O(|\nu|^{-1/2})$ than the spanwise continuum result (4.11) and the continuum ring result (5.8) – the solution can be interpreted as a two-dimensional continuum of stationary points $(\tilde{u}, \tilde{z})$ spread across the entire propeller source annulus.

Results are discussed in the following section for a range of azimuthal mode numbers and for both straight and swept propellers, including the specific case addressed here ($\nu = 0$, $\Gamma^{\dagger\prime}(z) = 0$), and detailed comparisons are made with full numerical calculations across all observer radiation angles, including observers located on the rotor axis, which bear out the asymptotic analyses both qualitatively and quantitatively.

Here, then, it is sufficient to point out again the power of the asymptotic approach in producing reduced-order formulae that contain no double integrals or special functions and can thus be evaluated extremely rapidly. Yet (as is shown in the next section) these formulae are accurate and, moreover, can explain the variations in the directivity of the far-field sound for zero, low and high azimuthal mode numbers as well as the underlying physics that drives the noise generation process.

## 6. Numerical verification of the asymptotic solutions

In this section, we present the interaction tones produced by two different 'verification' propeller designs. Predictions are made, firstly, using an 'exact' numerical calculation of (2.31) and, secondly, using the leading-order asymptotic formulae presented in §§ 3 and 5; the two are presented and compared in order to assess the validity of the asymptotic expressions. We emphasise here that, although the asymptotic solutions are largely simple algebraic formulae, we are still using them to obtain absolute – rather than relative – levels in the comparisons.

The advanced open rotor considered in the examples presented in this paper has, unless otherwise stated, the following design parameters: $M_x = 0.1998$, $M_{T_1} = 0.7074$, $M_{T_2} = 0.7132$, $D = 0.6096$ m, $R_h = D/5$, $g = 0.2394D$, $c_1 = c_2 = 0.1D$ and $C_{D_1} = 0.02$ where $C_{D_1}$ is the sectional drag coefficient of the front propeller. The observer is located at $R_e = 1$ m and the ambient speed of sound and air density are 344.4 m s$^{-1}$ and 1.1192 kg m$^{-3}$ respectively. These particular parameters are based on a design published in Whitfield, Mani & Gliebe (1990*a*,*b*) – which is assumed to be representative of a state-of-the-art contra-rotating propeller design at that time –

and are used in the remainder of this paper, apart from special cases for which, of necessity, we redefine certain values. However, by far the most important parameters are the blade numbers which will be used in our asymptotic analyses. In order for our results to be representative of the latest open rotor configurations, therefore, we have taken examples from tests of more recent open rotors which have been discussed by Parry *et al.* (2012). Little aerodynamic or geometrical information is available there but the blade numbers are given as $B_1 = 12$, $B_2 = 9$ and we have elected to use those values. It is, of course, necessary to supply both the numerical and asymptotic radiation formulae with the values of the unsteady lift. To obtain these values we have modelled the wake deficit velocity from each upstream propeller blade as a delta function gust aligned with the negative $X_1$-direction with magnitude $\overline{u}' = U_{r_1}\Theta\delta(Y_1)$, where $\Theta = C_{D_1}c_1/2$ is the momentum thickness of the wake. (Such a gust produces qualitatively similar results to the more realistic wake profiles which we have tested using this method (such as those described in Parry 1988, 1997) but removes the effect of the wake profile and its development on the results.) The amplitude function $G(z)$ is given by either (2.44)–(2.45) for straight (or slightly swept) blade cases or (2.46)–(2.47) for cases in which the sweep is such that the gust interaction is sub-critical. The main intent is that precisely the same values are used for both the full numerical calculations and the asymptotic approximations.

### 6.1. *Straight-bladed propellers*

The first case which is considered is a blade design for which $\Gamma'(z) = 0$. Such a design is achieved by setting the leading-edge sweep of the propeller blades equal to zero and will be referred to as 'straight bladed'. For this case the sound radiation is dominated by interior stationary points at $\tilde{z} = |z^*|$ and $\tilde{u} = \mathrm{sgn}(z^*)\pi/2$ and caustic interior stationary points are not possible.

From § 3.1 the leading-order asymptotic contribution from interior stationary points on a straight-bladed propeller are given by (3.8). In order to best show the power of the asymptotics, we also include the leading-order contributions from the boundary critical points which are given by (3.12).

Figures 6–8 plot the far-field directivity, in terms of sound pressure level (SPL) versus $\theta_e$, for a number of different tones. Here we feel it is important to show results for a number of different azimuthal mode orders that occur in practice, and that represent different asymptotic regimes. For the dominant interior stationary points we know, from the introduction to § 3, that the assumptions underpinning the asymptotic approach are violated when the interior critical points are located close to the outer ring ($z = 1$), or inner ring ($z = z_h$), of the source annulus where the solution drops to half its value. For the results presented here, solutions are thus excluded within 2.5° of the angle at which the interior stationary point is located on the inner or outer ring. The asymptotics governing the boundary critical point solutions also become invalid close to locations where the leading-order solution switches from a boundary critical point solution to an interior stationary point solution. In these transition regions, where the solution switches from one which is interior stationary point dominated to one which is boundary critical point dominated, the solution diverges and, clearly, close to these points the agreement between the asymptotic and numerical solutions will become poor. A singularity is to be expected as it represents the point at which an interior stationary point enters (or exits) the domain (the propeller source annulus). An interior stationary point requires both the first-order derivatives $\hat{\Phi}_{0,1}$ and $\hat{\Phi}_{1,0}$ to be zero. In particular, an interior stationary point at the

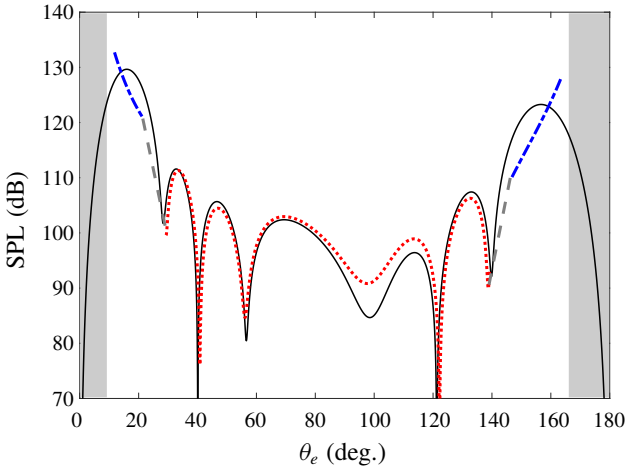


FIGURE 6. (Colour online) Plot of SPL versus $\theta_e$ for the $n_1 = 1$, $n_2 = 1$ tone with $\nu = -3$. The solid line denotes numerical solutions whilst interior stationary point solutions are denoted by the dash-dot lines and boundary critical point solutions are denoted by the dotted line. The shaded regions correspond to locations where no critical point exists and the grey dashed lines denote interpolated levels within the exclusion zones.

tip requires $\hat{\Phi}_{0,1} = 0$ at $\tilde{z} = 1$; as the boundary critical point solution contains a factor $\hat{\Phi}_{0,1}$ in the denominator, the solution diverges there – see (3.12).

It is important to point out that the asymptotic approach can be extended to construct uniformly valid asymptotic expansions in these different transition regions, as did Crighton & Parry (1992) for single-rotating propellers. In our case the solution in the transition zones would then be expressed in terms of Fresnel integrals and Airy functions. Whilst the derivation of the precise form of the solution in these regions is straightforward, it is laborious and beyond the scope of the present paper. However, these transition regions are, clearly, known *a priori* (they occur when $z^* = 1$ or $z^* = z_h$). Consequently, in order to provide a solution that can be used in practice, we have defined small neighbourhoods, that extend merely 5° either side of the singularity, where the solution is not calculated. With the application of the exclusion zones, the agreement between the leading-order asymptotic solutions and the numerical calculations is reasonable (to within a few decibels). For the practical application of our solution, we have used linear interpolation between the leading-order asymptotic solutions, across the exclusion zones, to estimate the noise levels there. The interpolation levels are shown as grey dashed lines in the figures.

In figure 6, the tone has $n_1 = 1$, $n_2 = 1$ so that $\nu = -3$. For this case, the asymptotic calculations produce reasonably accurate results when compared to full numerical evaluations. The sound field for this tone is dominated by radiation in directions close to – but not along – the flight axis. Specifically, the plot shows that the highest levels correspond to the interior stationary points which are spread broadly over a narrow angular range just away from the axis. In fact, the analysis of § 5.1, applied to the current geometry, would suggest that the interior stationary points should only occur at observer positions in the forward arc for which $9° < \theta_e < 23°$, in general agreement with the results of figure 6.

The results in figure 7 are for a tone with $n_1 = 3$, $n_2 = 2$ so that $\nu = -18$. The far-field sound is completely dominated in almost all radiation directions by the interior

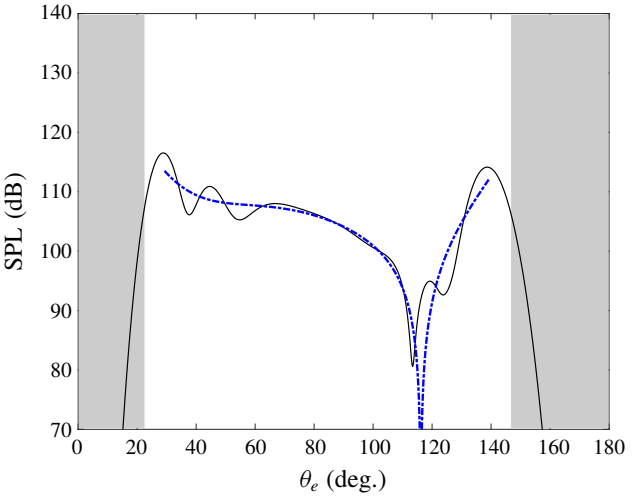


FIGURE 7. (Colour online) Plot of SPL versus $\theta_e$ for the $n_1 = 3$, $n_2 = 2$ tone with $\nu = -18$. The solid line denotes numerical solutions whilst interior stationary point solutions are denoted by the dash-dot line. The shaded regions correspond to locations where no critical point exists.

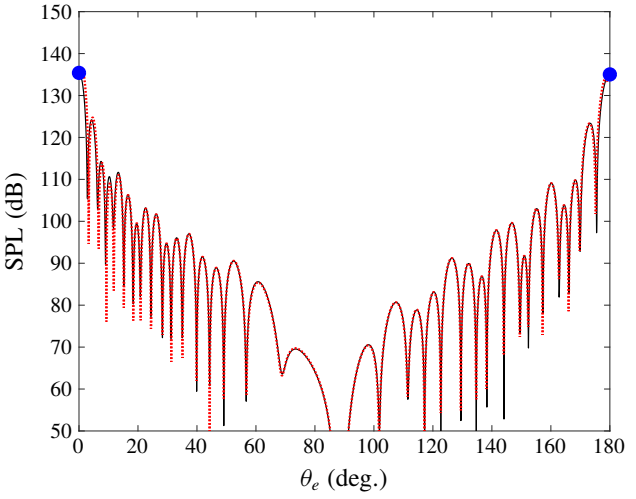


FIGURE 8. (Colour online) Plot of SPL versus $\theta_e$ for the $n_1 = 3$, $n_2 = 4$ tone with $\nu = 0$. The solid line denotes the numerical solutions whilst the dotted line denotes the asymptotic solutions. These are boundary critical points except on-axis where the asymptotic solutions are given by (5.10) and are plotted as solid circles.

stationary points, apart from the region close to the axis where $|z^*| > 1$ and the levels are very low. There is good agreement (to within a few dB) between the full numerical calculations and the asymptotics.

Finally, we consider a tone for which the azimuthal mode number $\nu = 0$ and the asymptotic solutions used in this special case are given in appendix D, except for the extreme (on-axis) angles which are discussed in § 5.2. The results are shown in

figure 8. Away from the axis all the (asymptotic) solutions are boundary critical points and there is very good agreement – to within 1 dB for most of the angular range – between the numerics and the asymptotics. Near to the axis, however, there is a very rapid rise in the noise levels to a maximum value on axis, precisely as suggested by the asymptotic analysis of § 5.2 which argues that the sound on axis represents a higher-order solution which originates from a two-dimensional continuum of interior stationary points. Here the numerics and asymptotics agree to within a few decibels.

### 6.2. *Swept propellers*

The second case we consider is that of an engine with downstream blades that have leading-edge sweep defined as a simple linear function: $\bar{s}_L = \lambda M_{r_2}(z - z_h)$, where we set $\lambda = 1/2$.

For these swept leading edges we have

$$\Gamma'(z) = \frac{\lambda}{z^* \sin\theta_e}, \tag{6.1}$$

so that $\Gamma'(z)$ is independent of $z$. Interior stationary points occur when

$$\tilde{z}^2 = \frac{z^{*2}}{1 - [\lambda \operatorname{cosec}\theta_e]^2}. \tag{6.2}$$

With this design we now consider, as in § 6.1, the directivities, SPL versus $\theta_e$, for low-, high- and zero-order azimuthal modes.

As in § 6.1, we omit solutions in the transition zones, 5° either side of any singularity, at which boundary critical points appear or disappear (enter or leave the propeller source domain) and within 2.5° of the angle at which the interior point is located at the hub or tip.

The results in figure 9 show the $n_1 = 1$, $n_2 = 1$ tone which has azimuthal mode order $\nu = -3$. Here, we see, by comparison with figure 6 for the straight-bladed case, that the effect of leading-edge sweep is to change the observer locations over which interior stationary points occur, producing a corresponding increase in the sound levels over that range – precisely as predicted by the asymptotics and discussed in § 5.1. Specifically, the interior stationary point solutions for the swept case in figure 9 occur further away from the axis than those of the straight-bladed case and lie in the 30°–40° range, approximately, over which the noise levels are around 10 dB higher than the straight-bladed case. There are similar results towards the rearward facing flight axis. The results also continue to show the generally good agreement between the asymptotic solutions and the full numerical calculations. However, note for this case that there is a large exclusion zone between 19° and 34° which is caused by two separate singularities: one associated with the hub (at 24°) and one with the tip (at 31.8°).

The solution in figure 10 is the $n_1 = 3$, $n_2 = 2$ tone with $\nu = -18$. For this case much of the radiation occurs away from the axis where it is governed mainly by interior stationary points but with two regions – located approximately around 30° and 140° – governed by boundary critical point solutions. There is, once again, good agreement (to within a few decibels) between the leading-order asymptotic solutions and the numerical calculations, except at angles close to the interior stationary-boundary critical point transition regions (and close to $|z^*| > 1$) where the assumptions underpinning the asymptotic solution become questionable; in these

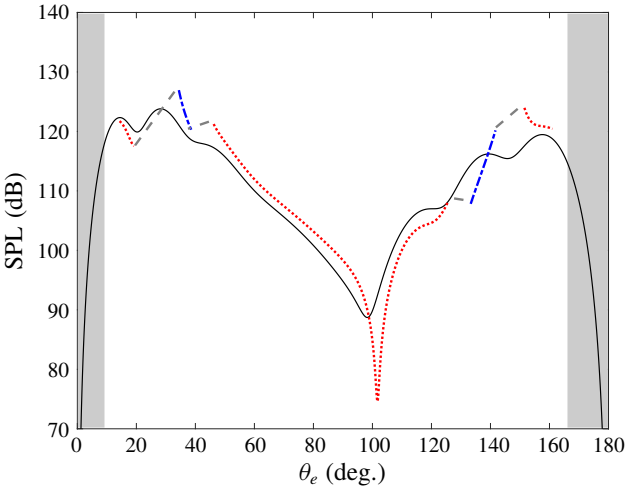


FIGURE 9. (Colour online) Plot of SPL versus $\theta_e$ for the $n_1 = 1$, $n_2 = 1$ tone with $\nu = -3$. The solid line denotes numerical solutions whilst interior stationary point solutions are denoted by the dash-dot lines and boundary critical point solutions are denoted by the dotted line. The shaded regions correspond to locations where no critical point exists and the grey dashed lines denote interpolated levels within the exclusion zones.

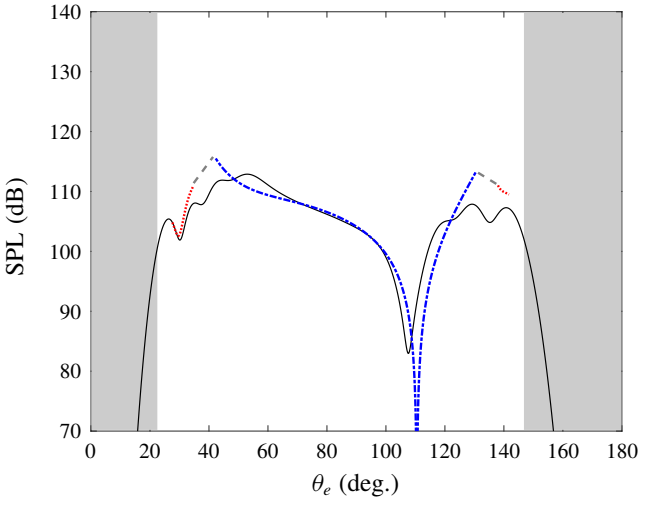


FIGURE 10. (Colour online) Plot of SPL versus $\theta_e$ for the $n_1 = 3$, $n_2 = 2$ tone with $\nu = -18$. The solid black line denotes numerical solutions whilst interior stationary point solutions are denoted by the dash-dot line and boundary critical point solutions are denoted by the dotted lines. The shaded regions correspond to locations where no critical point exists and the grey dashed lines denote interpolated levels within the exclusion zones.

regions, as before, we have omitted the formal asymptotic solution and interpolated. Comparing the result in figure 10 with that for the straight-bladed case in figure 7, we see that sweep is beneficial for this tone. The effect of sweep is to remove the

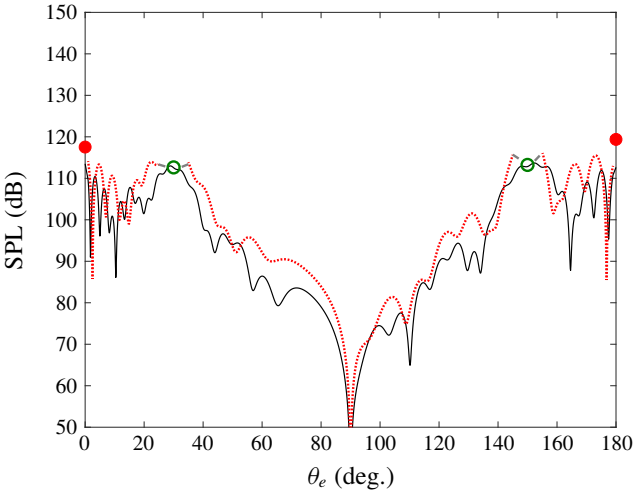


FIGURE 11. (Colour online) Plot of SPL versus $\theta_e$ for the $n_1 = 3$, $n_2 = 4$ tone with $\nu = 0$. The solid black line denotes numerical solutions whilst the dotted line denotes an asymptotic solution. These are boundary critical points given by (D 13) except for the critical solutions given by (D 12) and plotted as hollow circles and the on-axis result given by (D 16) and plotted as solid circles. The grey dashed lines denote interpolated levels within the exclusion zones.

interior stationary point solutions over two regions of around 20° range, towards the forward and rearward flight axes, and replace them with lower-order boundary critical point solutions such that the radiated sound levels are reduced by around 10 dB in these regions.

Finally, we show the solution in figure 11 for the $n_1 = 3$, $n_2 = 4$ tone with $\nu = 0$. For this zero-order mode, with the sweep defined by $\bar{s}_L = (1/2)M_{r_2}(z - z_h)$, it is clear from (5.6) that the design becomes critical at the point at which $\sin\theta_e = 1/2$ so that critical solutions exist in the radiated field at $\theta_e = 30°$ and 150°. The asymptotic evaluation of the sound radiation integral for these angles is given in appendix D and the results indicated in figure 11 by a hollow circle. Elsewhere, as the sweep is linear, there are no interior stationary points and the sound radiation is governed by boundary critical points – for which the solutions have, once again, been omitted close to the singular point. Along the axes, the asymptotic solution is given by (5.9) and, as discussed in § 5.2, represents a continuum ring of boundary critical points with an asymptotic solution of $O(\eta^{-1})$; solid circles are used to indicate the resultant on-axis levels. The asymptotic solutions agree with the numerical results typically to within a few decibels.

In this section we have shown that the asymptotic approach is able to identify particular features of a contra-rotating propeller's sound generation and radiation process and, moreover, that the leading-order asymptotic solutions are able to produce accurate and quantitative predictions of the directivities of tones from a representative modern propeller configuration provided the assumptions underpinning the asymptotic expansions are satisfied. We also showed that the leading-order boundary critical point expressions become singular in the transition region so that the asymptotic expressions become inaccurate there. The agreement in these zones could be improved by the application of uniform asymptotics but here, in order to produce a solution which can

be used practically, we have defined exclusion zones around the discontinuities and interpolated across them. To demonstrate the applicability of the asymptotic approach, we have chosen tones from two different propeller blade designs, one with a straight leading edge and one with leading-edge sweep, and compared the analyses for high-, low- and zero-order modes. The results demonstrate the power of the asymptotic approach – not just in the speed of the calculations but also in the accuracy of the resultant solution. The agreement is all the more remarkable bearing in mind the simplicity of the asymptotic expressions, which are largely algebraic, and the fact that we have included here only the leading-order term.

## 7. Conclusions

In this paper the generation and radiation of interaction tones from a contra-rotating propeller has been considered. The general far-field radiation equations in the frequency domain utilised here are well known (see Hanson 1985), although the inputs include the unsteady lift coefficients which are generally unknown *a priori*. Here we have obtained those lift coefficients using a generic Fourier description of the incident wakes along with a swept blade response function that accounts for both super-critical and sub-critical gust response. Then, by recasting the acoustic radiation formula as a double integral over a nominal source annulus, it was shown how to evaluate the radiation formula using asymptotic techniques for double integrals using the assumption that the number of blades was large on both front and rear rows. The leading-order result for each tone either came from interior stationary points or, alternatively, a number of (lower-order) boundary critical points – representing the dominant source locations on the propeller source annulus – and these tonal results comprised largely of simple algebraic expressions. The locations of the interior stationary points are given by the solutions to (3.4) and represent points at which the rapidly varying phase, around the propeller source annulus, becomes stationary and thus not self-cancelling – unlike that from the remainder of the surface. A detailed discussion of the role of these stationary points was given in § 3.1. In addition, the radial locations were shown to be entirely consistent with an unsteady aerodynamic gust interaction calculation in that interior stationary points could not exist in regions where the gust interaction was sub-critical.

It was also shown, via the asymptotic approach, that sweep could be used to produce a critical design – which generated a continuum of interior stationary points on the source annulus that generated a higher-order solution. It was thus demonstrated that sweep had the potential to increase noise radiation significantly.

Additional asymptotic solutions were produced for tones of low and zero azimuthal order. For these cases, asymptotic analysis illustrated precisely how the sound field would be dominated by radiation in a small region close to the flight axis. For the specific case of zero circumferential order, it was found that the sound field was completely dominated by radiation along the axis (not just near to it). In this direction, a swept-blade design would produce high levels of radiation – equivalent to that from a critical design for a non-zero azimuthal mode order tone – with the radiation emanating from a ring of sources at a specific radius. A straight-bladed design produced the highest on-axis result of all, of order 1, with the entire propeller annulus (rather than a point or a line) contributing to the radiation.

Comparisons have been made between the asymptotic results and full numerical evaluations of the sound field using representative propeller geometry and aerodynamics. Those comparisons showed good agreement, both qualitatively and quantitatively,

between the two sets of results in terms of the far-field directivities for a number of tones. The exceptions are at the transition points between regions dominated by different types of solution: interior stationary points, boundary critical points and exponentially decaying ($|z^*| > 1$). At these transition points the asymptotic results diverge and, for reasons of practicality, we have omitted the results in small regions about the singularities and interpolated across them. Uniform asymptotic analyses could be employed to produce smooth and continuous solutions in these transition zones.

Throughout, we have demonstrated the remarkable power of the asymptotic approach: in its ability to produce extremely fast and reasonably accurate predictions; in the reduced one-line algebraic equations that illustrate, at once, how the magnitude of the radiation varies with design, tone and observer direction; and in its ability to demonstrate that sweep can lead to enhanced noise radiation.

## Appendix A. High-frequency evaluation of the amplitude function

The amplitude function $G(z)$ was introduced in § 2.3 with precise closed form expressions given by (2.44) and (2.46) for super-critical and sub-critical response, respectively. At high frequencies, entirely consistent with our high blade number assumption, and with the asymptotic analysis in § 3, the factors $\mathbb{L}_<$ and $\mathbb{L}_>$, given by (2.45) and (2.47), are $O(\nu)$ because, from (2.11) and (2.13), $k_x$ and $\sigma_2$ are also $O(\nu)$. We can thus use the asymptotic expansions

$$E(x) \sim \frac{\mathrm{e}^{\mathrm{i}(\pi/4)}}{\sqrt{2}} - \frac{\mathrm{i}\mathrm{e}^{\mathrm{i}(\pi/2)x^2}}{\pi x}, \quad \mathrm{erf}(x) \sim 1 - \frac{\mathrm{e}^{-x^2}}{\sqrt{\pi}x} \quad \text{as } x \to \infty \tag{A 1a,b}$$

to obtain the leading-order terms from (2.44) and (2.46) as

$$G(z) = M_{r_2} m_{n_1} \times \left[ \frac{1}{\sqrt{1 + \sqrt{M_{r_2}^2 - \tan^2 \Lambda}}} \frac{k_y}{\sqrt{\sigma_2 \mathbb{L}_<}} \right] \tag{A 2}$$

and

$$G(z) = M_{r_2} m_{n_1} \times \left[ \frac{\mathrm{e}^{-\mathrm{i}(\pi/4) + (\mathrm{i}/2)\tan^{-1}\sqrt{\tan^2 \Lambda - M_{r_2}^2}}}{[1 + (\tan^2 \Lambda - M_{r_2}^2)]^{1/4}} \frac{k_y}{\sqrt{\sigma_2 \mathbb{L}_>}} \right], \tag{A 3}$$

respectively. But, since from (2.35) $k_y$ is also $O(\nu)$, the terms in brackets in (A 2) and (A 3) are both $O(1)$ as $\nu \to \infty$ showing that, although the chordwise response decays exponentially away from the leading edge in the sub-critical gust interaction regions for which $\Lambda > \Lambda^*$, the leading-order contribution to the unsteady response – from the leading edge – is still of the same order of magnitude as that from a super-critical gust interaction and the net acoustic radiation remains governed by the interior and/or boundary critical points obtained in § 3.

## Appendix B. Interior stationary points of higher order

For cases where $\tilde{\Phi}_{2,0}\tilde{\Phi}_{0,2} = \tilde{\Phi}_{1,1}^2$ at an interior stationary point, the phase function has stationary points of higher order and the expression derived in § 3.1 is no longer applicable. For such a case we expand $\Phi(u, z)$ in a Taylor series about the

stationary point $z=\tilde{z}$, $u=\tilde{u}$. Including third-order terms we find, after using the simple transformation defined by (3.6) that

$$\Phi(u,z)=c_{0,0}+\tfrac{1}{2}c_{2,0}U^2+\tfrac{1}{2}c_{1,2}UZ^2+\tfrac{1}{2}c_{2,1}U^2Z+\tfrac{1}{6}c_{0,3}Z^3+\tfrac{1}{6}c_{3,0}U^3+\cdots, \tag{B 1}$$

where

$$\left.\begin{aligned} &c_{0,0}=\tilde{\Phi}_{0,0},\quad c_{2,1}=\tilde{\Phi}_{2,1}-\frac{\tilde{\Phi}_{3,0}\tilde{\Phi}_{1,1}}{\tilde{\Phi}_{2,0}},\quad c_{1,2}=\tilde{\Phi}_{1,2}-2\frac{\tilde{\Phi}_{1,1}\tilde{\Phi}_{2,1}}{\tilde{\Phi}_{2,0}}+\frac{\tilde{\Phi}_{1,1}^2\tilde{\Phi}_{3,0}}{\tilde{\Phi}_{2,0}^2},\\ &c_{2,0}=\tilde{\Phi}_{2,0},\quad c_{3,0}=\tilde{\Phi}_{3,0},\quad c_{0,3}=\tilde{\Phi}_{0,3}-3\frac{\tilde{\Phi}_{1,1}\tilde{\Phi}_{1,2}}{\tilde{\Phi}_{2,0}}+3\frac{\tilde{\Phi}_{1,1}^2\tilde{\Phi}_{2,1}}{\tilde{\Phi}_{2,0}^2}-\frac{\tilde{\Phi}_{1,1}^3\tilde{\Phi}_{3,0}}{\tilde{\Phi}_{2,0}^3}. \end{aligned}\right\} \tag{B 2}$$

We introduce the additional transformation

$$\zeta=Z+\frac{c_{1,2}}{c_{0,3}}U,\quad \upsilon=U, \tag{B 3a,b}$$

for which the Jacobian is once again unity, so that, after a little manipulation,

$$\begin{aligned}\Phi(u,z)\;=\;&c_{0,0}+\frac{1}{2}c_{2,0}\upsilon^2\left[1+\frac{c_{3,0}c_{0,3}^2-3c_{1,2}c_{2,1}c_{0,3}+2c_{1,2}^3}{3c_{2,0}c_{0,3}^2}\upsilon+\frac{c_{2,1}c_{0,3}-c_{1,2}^2}{c_{2,0}c_{0,3}}\zeta\right]\\&+\frac{1}{6}c_{0,3}\zeta^3+\cdots.\end{aligned} \tag{B 4}$$

The integral is then, to leading order, given by

$$I_{n_1,n_2}\sim\frac{\tilde{G}}{2\pi\mathrm{i}^{\nu}}\exp\{\mathrm{i}\nu c_{0,0}\}\int_{-\infty}^{\infty}\exp\left\{\mathrm{i}\frac{\nu}{2}c_{2,0}\upsilon^2\right\}\mathrm{d}\upsilon\int_{-\infty}^{\infty}\exp\left\{\mathrm{i}\frac{\nu}{6}c_{0,3}\zeta^3\right\}\mathrm{d}\zeta, \tag{B 5}$$

which evaluates as

$$I_{n_1,n_2}\sim\frac{\Gamma(1/3)\tilde{G}}{\pi^{1/2}6^{1/6}|c_{2,0}|^{1/2}|c_{0,3}|^{1/3}}\frac{\exp\left\{\mathrm{i}\nu\left(c_{0,0}-\frac{\pi}{2}\right)+\mathrm{i}\frac{\pi}{4}\mathrm{sgn}(\nu)\mathrm{sgn}(c_{2,0})\right\}}{|\nu|^{5/6}}. \tag{B 6}$$

## Appendix C. Critical sweep – simplified solutions

In this appendix we consider the critical sweep design, with the sweep given by (4.7) and (4.8) and the acoustic radiation given by (4.11). For a simple case in which the amplitude function $G(z)$ is taken to be approximately constant, with $G(z)=G_0$, we can evaluate the integral (4.11) as (see Gradshteyn & Ryzhik 2014)

$$\begin{aligned}I_{n_1,n_2}\;\sim\;&\frac{|z^*|G_0}{\sqrt{2\pi|\nu|}}\exp\left\{\mathrm{i}\nu D-\mathrm{i}\frac{\pi}{4}\right\}\left\{F\left(\gamma_1,\frac{1}{\sqrt{2}}\right)-2E\left(\gamma_1,\frac{1}{\sqrt{2}}\right)\right.\\&\left.+\frac{2(1-z^{*2})^{1/4}}{\sqrt{|z^*|}\left[|z^*|+\sqrt{1-z^{*2}}\right]}\right\},\end{aligned} \tag{C 1}$$

where $F$ and $E$ are elliptic integrals of the first and second kind, respectively, and

$$\gamma_1 = \cos^{-1}\left(\frac{|z^*|-\sqrt{1-z^{*2}}}{|z^*|+\sqrt{1-z^{*2}}}\right). \tag{C 2}$$

For the case in which the sonic radius lies inside the hub ($|z^*| < z_h$) we get

$$\begin{aligned} I_{n_1,n_2} \sim \frac{|z^*|G_0}{\sqrt{2\pi\nu}}\exp\left(\mathrm{i}\nu D - \mathrm{i}\frac{\pi}{4}\right)\left[F\left(\gamma_1, \frac{1}{\sqrt{2}}\right) - 2E\left(\gamma_1, \frac{1}{\sqrt{2}}\right)\right. \\ + \frac{2(1-z^{*2})^{1/4}}{\sqrt{|z^*|}\left(|z^*|+\sqrt{1-z^{*2}}\right)} - F\left(\gamma_2, \frac{1}{\sqrt{2}}\right) + 2E\left(\gamma_2, \frac{1}{\sqrt{2}}\right) \\ \left. - \frac{2z_h(z_h^2-z^{*2})^{1/4}}{\sqrt{|z^*|}\left(|z^*|+\sqrt{z_h^2-z^{*2}}\right)}\right], \end{aligned} \tag{C 3}$$

where

$$\gamma_2 = \cos^{-1}\left(\frac{1-\sqrt{\dfrac{z_h^2}{z^{*2}}-1}}{1+\sqrt{\dfrac{z_h^2}{z^{*2}}-1}}\right). \tag{C 4}$$

## Appendix D. Asymptotic expressions for $\nu = 0$

For the case where $\nu = 0$ (so that $n_2B_2 = n_1B_1$ with $n_2B_2 \to \infty$) we use the formally large parameter $\eta = n_1B_1M_{T_1} + n_2B_2M_{T_2} = n_2B_2(M_{T_1} + M_{T_2})$ and

$$I_{n_1,n_2} = \frac{1}{2\pi}\int_{z_h}^{1}\int_{-\pi}^{\pi} G(z)\exp\{\mathrm{i}\eta\Phi^\dagger(u,z)\}\,\mathrm{d}u\,\mathrm{d}z, \tag{D 1}$$

where $G(z)$ is defined as before and $\Phi^\dagger(u,z)$ is a phase function which is defined as

$$\Phi^\dagger(u,z) = \frac{z}{z^\dagger}\cos u - \Gamma^\dagger(z), \tag{D 2}$$

where

$$z^\dagger = \frac{(1-M_x\cos\theta_e)}{\sin\theta_e}, \tag{D 3}$$

and

$$\Gamma^\dagger(z) = \frac{1}{(1-M_x\cos\theta_e)}\frac{\bar{s}_L}{M_{r_2}} + \Lambda^\dagger\bar{g}\frac{M_{T_1}}{M_x}, \tag{D 4}$$

with $\Lambda^\dagger = n_2B_2/\eta = 1/(M_{T_1} + M_{T_2}) = O(1)$. For $\eta \to \infty$ we can evaluate the double integral asymptotically using the methods described in § 3 yielding the following results:

(i) Interior critical points occur at $u = 0$ and $u = \pi$ and at radial locations determined by the solution to $\Gamma^{\dagger\prime}(\tilde{z}) = 1/z^\dagger$ for $u = 0$ (where $\tilde{\Phi}^\dagger_{2,0} = -\tilde{z}/z^\dagger$, $\tilde{\Phi}^\dagger_{0,2} = -\Gamma^{\dagger\prime\prime}(\tilde{z})$ and

$\tilde{\Phi}^{\dagger}_{1,1} = 0$) and $\Gamma^{\dagger\prime}(\tilde{z}) = -1/z^{\dagger}$ for $u = \pi$ (where $\tilde{\Phi}^{\dagger}_{2,0} = \tilde{z}/z^{\dagger}$, $\tilde{\Phi}^{\dagger}_{0,2} = -\Gamma^{\dagger\prime\prime}(z)$ and $\tilde{\Phi}^{\dagger}_{1,1} = 0$). Following the analysis presented in §§ 3.1 and 5.2, we obtain

$$I_{n_1,n_2} \sim \frac{\tilde{G}}{\eta\sqrt{|\tilde{\Phi}^{\dagger}_{2,0}\tilde{\Phi}^{\dagger}_{0,2}|}} \exp\left\{\mathrm{i}\eta\tilde{\Phi}^{\dagger}_{0,0} + \mathrm{i}\frac{\pi}{4}\mathrm{sgn}(\tilde{\Phi}^{\dagger}_{2,0})[1 + \mathrm{sgn}(\tilde{\Phi}^{\dagger}_{2,0}\tilde{\Phi}^{\dagger}_{0,2})]\right\}. \tag{D 5}$$

We see that, apart from the on-axis cases, which were discussed in § 5.2, for an open rotor with no leading-edge sweep or lean (such that $\Gamma^{\dagger\prime}(z) = 0$), only boundary critical points may occur.

(ii) Boundary critical points always occur at $u = \hat{u}_{+} = 0$ and $u = \hat{u}_{-} = \pi$ at both $z = 1$ and $z = z_h$. For the tip contributions we have

$$I^{\pm}_{n_1,n_2} \sim \pm\frac{\hat{G}\exp\left\{\mathrm{i}\eta\tilde{\Phi}^{\dagger}_{0,0} + \mathrm{i}\frac{\pi}{4}\mathrm{sgn}(\tilde{\Phi}^{\dagger}_{2,0})\right\}}{\mathrm{i}\sqrt{2\pi}\eta^{3/2}\sqrt{|\tilde{\Phi}^{\dagger}_{2,0}|}\tilde{\Phi}^{\dagger}_{0,1}}, \tag{D 6}$$

whilst for hub contributions we have

$$I^{\pm}_{n_1,n_2} \sim \frac{\hat{G}\exp\left\{\mathrm{i}\eta\tilde{\Phi}^{\dagger}_{0,0} + \mathrm{i}\frac{\pi}{4}\mathrm{sgn}(\tilde{\Phi}^{\dagger}_{2,0})\right\}}{\mathrm{i}^{-1}\sqrt{2\pi}\eta^{3/2}\sqrt{|\tilde{\Phi}^{\dagger}_{2,0}|}\tilde{\Phi}^{\dagger}_{0,1}}. \tag{D 7}$$

(iii) When the sweep is linear such that $\bar{s}_L = \lambda M_{r_2}(z - z_h)$, as was considered in § 6.2 for the case in which $\lambda = 1/2$, we have

$$\Gamma^{\dagger\prime}(z) = \frac{\lambda}{z^{\dagger}\sin\theta_e}, \tag{D 8}$$

and interior stationary points occur when $u = 0$ or $\pi$ and, respectively, $\theta_e = \pm\sin^{-1}\lambda$. Since (D 8) is satisfied for all $z$ there are interior stationary points at all radii and the solution is clearly critical. As boundary critical points also occur at $u = 0$ or $\pi$ we can write the phase function $\Phi^{\dagger}(u, z)$ at general points in the sound field, away from the axis, as

$$\Phi^{\dagger}(u, z) = \frac{z}{z^{\dagger}}\cos u - \Gamma^{\dagger}(z) = \frac{\lambda}{\sin\theta_e}\frac{z_h}{z^{\dagger}} + \left(1 - \frac{\lambda}{\sin\theta_e}\right)\frac{z}{z^{\dagger}} - \frac{1}{2}\frac{z}{z^{\dagger}}u^2 \tag{D 9}$$

by expanding near to $u = 0$. Equivalent solutions are obtained by expanding near to $u = \pi$. The radiation integral can now be written as

$$I_{n_1,n_2} = \frac{\exp\left(\mathrm{i}\eta\frac{\lambda}{\sin\theta_e}\frac{z_h}{z^{\dagger}}\right)}{2\pi}\int_{z_h}^{1} G(z)\exp\left[\mathrm{i}\eta\left(1 - \frac{\lambda}{\sin\theta_e}\right)\frac{z}{z^{\dagger}}\right]\int_{-\pi}^{\pi}\exp\left[-\frac{\mathrm{i}\eta}{2}\frac{z}{z^{\dagger}}u^2\right]\mathrm{d}u\,\mathrm{d}z, \tag{D 10}$$

with the inner integral over $u$ easily evaluated for large $\eta$ as

$$\sqrt{\frac{2\pi|z^{\dagger}|}{\eta z}}\exp\left(-\mathrm{i}\frac{\pi}{4}\mathrm{sgn}\, z^{\dagger}\right). \tag{D 11}$$

The outer integral is dependent on the value of $\theta_e$. For $\theta_e = \sin^{-1}\lambda$ it becomes simply, after combining with (D 11),

$$I_{n_1,n_2} = \sqrt{\frac{|z^\dagger|}{2\pi\eta}}\exp\left\{\mathrm{i}\eta\frac{z_h}{z^\dagger} - \mathrm{i}\frac{\pi}{4}\operatorname{sgn} z^\dagger\right\}\int_{z_h}^{1}\frac{G(z)}{\sqrt{z}}\,\mathrm{d}z, \tag{D 12}$$

which is $O(\eta^{-1/2})$ and is similar to the weighted integral solution (4.11) given for the critical design in § 4.2. Elsewhere, for $\theta_e \neq \sin^{-1}\lambda$ and away from the axis, we obtain

$$\begin{aligned} I_{n_1,n_2} \;=\; & \frac{1}{\sqrt{2\pi}}\exp\left(-\mathrm{i}\frac{3\pi}{4}\operatorname{sgn} z^\dagger + \mathrm{i}\eta\frac{\lambda}{\sin\theta_e}\frac{z_h}{z^\dagger}\right) \\ & \times\frac{|z^\dagger|^{3/2}}{\left(1-\dfrac{\lambda}{\sin\theta_e}\right)\eta^{3/2}}\left\{G(z)\exp\left[\mathrm{i}\eta\left(1-\frac{\lambda}{\sin\theta_e}\right)\frac{z}{z^\dagger}\right]\right\}_{z=z_h}^{z=1}, \end{aligned} \tag{D 13}$$

which is a typical boundary critical point solution of $O(\eta^{-3/2})$. On the propeller axis we have a simple linear definition of the phase function, for $\theta_e = 0$ or $\pi$, respectively,

$$\Phi^\dagger(u, z) = \frac{-\lambda(z - z_h)}{(1 \mp M_x)}. \tag{D 14}$$

As the phase function is independent of $u$ the radiation integral becomes, immediately,

$$I_{n_1,n_2} = \int_{z_h}^{1} G(z)\exp\left\{-\mathrm{i}\eta\frac{\lambda(z - z_h)}{(1 \mp M_x)}\right\}\mathrm{d}z, \tag{D 15}$$

which can be evaluated asymptotically to yield the endpoint contributions

$$I_{n_1,n_2} = \mathrm{i}\frac{(1 \mp M_x)}{\eta\lambda}\left[G(z)\exp\left\{-\mathrm{i}\eta\frac{\lambda(z - z_h)}{(1 \mp M_x)}\right\}\right]_{z=z_h}^{z=1}, \tag{D 16}$$

which are $O(\eta^{-1})$. The solution represents boundary contributions from the hub and tip which are normally $O(\eta^{-3/2})$; however, as they arise in (D 16) from every possible azimuthal angle, the result represents a continuum ring of boundary sources.

## REFERENCES


Adamczyk, J. J. 1974 Passage of a swept airfoil through an oblique gust. *J. Aircraft* **11**, 281–287.

Bleistein, N. & Handelsman, R. A. 1969 Uniform asymptotic expansions of double integrals. *J. Math. Analysis Applics.* **27**, 434–453.

Brady, C. W. 1951 Propellers for high powers and transonic speeds. In *Proceedings of the 3rd Anglo-American Aeronautical Conference, Brighton, UK, 4–7 September*, pp. 613–668.

Brandvik, T., Hall, C. A. & Parry, A. B. 2012 Angle-of-attack effects on counter-rotating propellers at take-off. In *ASME Turbo Expo 2012, Copenhagen, Denmark, 11–15 June. ASME Paper* GT2012-69901.

Bryan, G. H. 1920 The acoustics of moving sources with application to airscrews. *British ARC R & M No.* 584.

Carazo, A., Roger, M. & Omais, M. 2011 Analytical prediction of wake-interaction noise in counterrotation open rotors. In *17th AIAA/CEAS Aeroacoustics Conference (32nd AIAA Aeroacoustics Conference), Portland, OR, 5–8 June. AIAA Paper* 2011-2758.

CHAKO, N. 1965 Asymptotic expansions of double and multiple integrals occurring in diffraction theory. *J. Inst. Maths Applics.* **1**, 372–422.

COLIN, Y., BLANC, F., CARUELLE, B., BARROIS, F. & DJORDJEVIC, N. 2012*b* Computational strategy for predicting CROR noise at low-speed. Part II. Investigation of the noise sources computation with the chorochronic method. In *18th AIAA/CEAS Aeroacoustics Conference (33rd AIAA Aeroacoustics Conference), Colorado Springs, CO, 4–6 June*. *AIAA Paper* 2012-2222.

COLIN, Y., CARUELLE, B., NODE-LANGLOIS, T., OMAIS, M. & PARRY, A. B. 2012*a* Computational strategy for predicting CROR noise at low-speed. Part I. Review of the numerical methods. In *18th AIAA/CEAS Aeroacoustics Conference (33rd AIAA Aeroacoustics Conference), Colorado Springs, CO, 4–6 June*. *AIAA Paper* 2012-2221.

COLIN, Y., CARUELLE, B. & PARRY, A. B. 2012*c* Computational strategy for predicting CROR noise at low-speed. Part III. Investigation of noise radiation with the Ffowcs-Williams Hawkings analogy. In *18th AIAA/CEAS Aeroacoustics Conference (33rd AIAA Aeroacoustics Conference), Colorado Springs, CO, 4–6 June*. *AIAA Paper* 2012-2223.

COOKE, J. C. 1982 Stationary phase in two dimensions. *IMA J. Appl. Maths* **29**, 25–37.

COOPER, A. & PEAKE, N. 2005 Upstream-radiated rotor–stator interaction noise in mean swirling flow. *J. Fluid Mech.* **523**, 219–250.

COOPER, A. & PEAKE, N. 2006 Rotor-stator interaction noise in swirling flow: stator sweep and lean effects. *AIAA J.* **44**, 981–991.

CRIGHTON, D. G. & PARRY, A. B. 1991 Asymptotic theory of propeller noise. Part II. Supersonic single-rotation propeller. *AIAA J.* **29**, 2031–2037.

CRIGHTON, D. G. & PARRY, A. B. 1992 Higher approximations in the asymptotic theory of propeller noise. *AIAA J.* **30**, 3023–3039.

DALY, B. B. 1958 Noise level in fans. *J. Inst. Heating Ventilating Engng* **25**, 29–45.

DELATTRE, G. & FALISSARD, F. 2015 Influence of torque ratio on counter-rotating open-rotor interaction noise. *AIAA J.* **53**, 2726–2738.

DE LABORDERIE, J. & MOREAU, S. 2016 Prediction of tonal ducted fan noise. *J. Sound Vib.* **372**, 105–132.

ENVIA, E. 1994 Asymptotic theory of supersonic propeller noise. *AIAA J.* **32** (2), 239–246.

ENVIA, E. 2015 Aeroacoustic analysis of a high-speed open rotor. *Intl J. Aeroacoust.* **14** (3 & 4), 569–606.

ENVIA, E. & KERSCHEN, E. J. 1984 Noise produced by the interaction of a rotor wake with a swept stator blade. In *9th AIAA Aeroacoustics Conference, Williamsburg, VA, 10–15 October*. *AIAA Paper No.* 84-2326.

ENVIA, E. & KERSCHEN, E. J. 1986 Noise generated by convected gusts interacting with swept airfoil cascades. In *10th AIAA Aeroacoustics Conference, Seattle, WA, 9–11 July*. *AIAA Paper No.* 86-1872.

ENVIA, E. & KERSCHEN, E. J. 1990 Influence of vane sweep on rotor–stator interaction noise. *NASA CR* 187052.

FALISSARD, F. & DELATTRE, G. 2014 Investigation of counter rotating open rotor orthogonal blade/vortex interaction noise. In *20th AIAA/CEAS Aeroacoustics Conference, AIAA Aviation forum, Atlanta, GA, 16–20 June*. *AIAA Paper* 2014-2748.

FUSS, U. & PARRY, A. B. 2011 SAGE1 demonstrator: enabling open rotor technologies. In *20th ISABE Conference, Gothenburg, Sweden, 12–16 September*. *ISABE Paper* 2011-1305.

GAUTSCHI, G. 1970 Error function and Fresnel integrals. In *Handbook of Mathematical Functions with Formulas, Graphs, and Mathematical Tables (9th Printing)* (ed. M. Abramowitz & I. A. Stegun). Dover.

GLEGG, S. A. L. 1999 The response of a swept blade row to a three-dimensional gust. *J. Sound Vib.* **227** (1), 29–64.

GOLDSTEIN, M. E. 1976 *Aeroacoustics*. McGraw-Hill.

GRADSHTEYN, I. S. & RYZHIK, I. M. 2014 *Table of Integrals, Series, and Products*, 8th edn. (ed. D. Zwillinger & V. Moll). Academic.

GRAHAM, J. M. R. 1970 Lifting surface theory for the problem of an arbitrarily yawed sinuosoidal gust incident on a thin aerofoil in incompressible flow. *Aeronaut. Q.* **21**, 182–198.

GRASSO, G., CHRISTOPHE, J., SCHRAM, C. F. & VERSTRAETE, T. 2014 Influence of the noise prediction model on the aeroacoustic optimization of a contra-rotating fan. In *20th AIAA/CEAS Aeroacoustics Conference, Atlanta, GA, 16–20 June*. *AIAA Paper* 2014-2611.

GUTIN, L. 1936 On the sound field of a rotating propeller. *Physik. Zeitschr. der Sowjetunion* **9** (1), 57–71; (translated as 1948 *NACA Tech. Memo.* 1195).

HANSON, D. B. 1983 Compressible helicoidal surface theory for propeller aerodynamics and noise. *AIAA J.* **21** (6), 881–889.

HANSON, D. B. 1985 Noise of counter-rotation propellers. *J. Aircraft* **22** (7), 609–617.

HANSON, D. B. 2001 Theory for broadband noise of rotor and stator cascades with inhomogeneous inflow turbulence including effects of lean and sweep. *NASA CR*-2001-210762.

HANSON, D. B. & PARZYCH, D. J. 1993 Theory for noise of propellers in angular inflow with parametric studies and experimental verification. *NASA CR*-4499.

HARRIS, R. & CUTHBERTSON, R. D. 1987 UDF/727 flight test program. In *23rd AIAA/SAE/ASME/ASEE Joint Propulsion Conference, San Diego, CA, 29 June–2 July. AIAA Paper* 1987-1733.

HUBBARD, H. H. 1948. Sound from dual-rotating and multiple single-rotating propellers. *NACA Tech. Note* 1654.

JAOUANI, N., ROGER, M., THOMAS NODE-LANGLOIS, T. & SERRE, G. 2016 Effect of a model leading-edge vortex on the blade aerodynamic response for application to CROR tonal noise predictions. In *22nd AIAA/CEAS Aeroacoustics Conference, Lyon, France, 30 May–1 June*. *AIAA Paper* 2016-2744.

JONES, D. S. & KLINE, N. 1958 Asymptotic expansion of multiple integrals and the method of stationary phase. *J. Math. Phys.* **37**, 1–28.

KINGAN, M. J. 2014 Advanced open rotor noise prediction. *Aeronaut. J.* **118** (1208), 1125–1135.

KINGAN, M. J., EKOULE, C. E., PARRY, A. B. & BRITCHFORD, K. 2014 Analysis of advanced open rotor noise measurements. In *20th AIAA/CEAS Aeroacoustics Conference, Atlanta, GA, 16–20 June*. *AIAA Paper* 2014-2745.

KINGAN, M. J. & SELF, R. 2009 Counter-rotation propeller tip vortex interaction noise. In *15th AIAA/CEAS Aeroacoustics Conference (30th AIAA Aeroacoustics Conference), Miami, FL, 11–13 May. AIAA Paper* 2009-3135.

LYNAM, E. J. H. & WEBB, H. A. 1919 The emission of sound by airscrews. *British ARC R & M No.* 624.

METZGER, F. B. & ROHRBACH, C. 1979 Aeroacoustic design of the propfan. In *5th Aeroacoustics Conference, Seattle, WA, 12–14 March*. *AIAA Paper* 1979-0610.

MOREAU, S., QUAGLIA, M. E. & FERNANDO, R. 2015 A 3D analytical approach for open rotor blade vortex interaction (bvi) tonal noise. In *21st AIAA/CEAS Aeroacoustics Conference, Dallas, TX, 22–26 June*. *AIAA Paper* 2015-2984.

PARKER, R. & LATHOUD, M. 2010 Green aeroengines: technology to mitigate aviation impact on environment. *Proc. Inst. Mech. Engng, Part C: J. Mech. Engng Sci.* **224** (3), 529–538.

PARRY, A. B. 1988 Theoretical prediction of counter-rotating propeller noise. PhD thesis, Department of Applied Mathematical Studies, University of Leeds.

PARRY, A. B. 1995 The effect of blade sweep on the reduction and enhancement of supersonic propeller noise. *J. Fluid Mech.* **293**, 181–206.

PARRY, A. B. 1997 Modular prediction scheme for blade row interaction noise. *J. Propul. Power* **13** (3), 334–341.

PARRY, A. B., BRITCHFORD, K. M., KINGAN, M. J. & SURESHKUMAR, P. 2012 Aeroacoustic tests of isolated open rotors at high speed. In *18th AIAA/CEAS Aeroacoustics Conference (33rd AIAA Aeroacoustics Conference), Colorado Springs, CO, 4–6 June*. *AIAA Paper* 2012-2220.

PARRY, A. B. & CRIGHTON, D. G. 1989*a* Prediction of counter-rotation propeller noise. In *12th Aeroacoustics Conference, San Antonio, TX, April 10–12*. *AIAA Paper* 89-1141.

PARRY, A. B. & CRIGHTON, D. G. 1989*b* Asymptotic theory of propeller noise. I. Subsonic single-rotation propeller. *AIAA J.* **27**, 1184–1190.

PARRY, A. B., KINGAN, M. & TESTER, B. J. 2011 Relative importance of open rotor tone and broadband noise sources. In *17th AIAA/CEAS Aeroacoustics Conference (33rd AIAA Aeroacoustics Conference), Portland, OR, 5–8 June*. *AIAA Paper* 2011-2763.

PARRY, A. B. & VIANELLO, S. 2012 A project study of open rotor noise. *Intl J. Aeroacoust.* **11**, 247–258.

PEAKE, N. & BOYD, W. K. 1993 Approximate method for the prediction of propeller noise near-field effects. *J. Aircraft* **30** (5), 603–610.

PEAKE, N. & CRIGHTON, D. G. 1991*a* Lighthill quadrupole radiation in supersonic propeller acoustics. *J. Fluid Mech.* **223**, 363–382.

PEAKE, N. & CRIGHTON, D. G. 1991*b* An asymptotic theory of nearfield propeller acoustics. *J. Fluid Mech.* **232**, 285–301.

PETERS, A. & SPAKOVSZKY, Z. S. 2010 Rotor interaction noise in counter-rotating propfan propulsion systems. In *ASME Turbo Expo 2010, Glasgow, UK, 14–18 June*. *ASME Paper* GT2010-22554.

QUAGLIA, M. E., LÉONARD, T., MOREAU, S. & ROGER, M. 2017 3D analytical model for orthogonal blade–vortex interaction noise. *J. Sound Vib.* **399**, 104–123.

QUAGLIA, M. E., MOREAU, S., ROGER, M. & FERNANDO, R. 2016 A preliminary semi-empirical approach for CROR noise modelling. In *22nd AIAA/CEAS Aeroacoustics Conference*. *AIAA Paper* 2016-2743.

ROGER, M. & CARAZO, A. 2010 Blade-geometry considerations in analytical gust-airfoil interaction noise models. In *16th AIAA/CEAS Aeroacoustics Conference, Stockholm, Sweden, 7–9 June*. *AIAA Paper 2010-3799*.

ROGER, M., SCHRAM, C. & MOREAU, S. 2012 On open rotor blade–vortex interaction noise. In *18th AIAA/CEAS Aeroacoustics Conference (33rd AIAA Aeroacoustics Conference), Colorado Springs, CO, 4–6 June. AIAA Paper* 2012-2216.

ROGER, M., SCHRAM, C. & MOREAU, S. 2014 On vortex-airfoil interaction noise including span-end effects, with application to open-rotor aeroacoustics. *J. Sound Vib.* **333**, 283–306.

ROHRBACH, C. & METZGER, F. B. 1975 The Prop-Fan – a new look in propulsors. In *2nd Aeroacoustics Conference, Hampton, VA, 24–26 March*. *AIAA Paper* 75-1208.

SHARMA, A. & CHEN, H. 2013 Prediction of aerodynamic tonal noise from open rotors. *J. Sound Vib.* **332**, 3832–3845.

SOHONI, N. G., HALL, C. A., BRANDVIK, T. & PARRY, A. B. 2015 Prediction and measurement of unsteady blade surface pressures on an open rotor. In *ASME Turbo Expo 2015, Montreal, Canada, 15–19 June*. *ASME Paper* GT2012-42334.

SOULAT, L., KERNEMP, I., SANJOSE, M., MOREAU, S. & FERNANDO, R. 2013 Assessment and comparison of tonal noise models for counter-rotating open rotors. In *19th AIAA/CEAS Aeroacoustics Conference, Berlin, Germany, 27–29 May*. *AIAA Paper* 2013-2201.

SOULAT, L., KERNEMP, I., SANJOSE, M., MOREAU, S. & FERNANDO, R. 2016 Numerical assessment of the tonal noise of counter-rotating open rotors at approach. *Intl J. Aeroacoust.* **15**, 23–40.

STÜRMER, A. & YIN, J. 2009 Low-speed aerodynamics and aeroacoustics of CROR propulsion systems. In *15th AIAA/CEAS Aeroacoustics Conference (30th AIAA Aeroacoustics Conference), Miami, FL, 11–13 May*. *AIAA Paper* 2009-3134.

STÜRMER, A., MARQUEZ GUTIERREZ, C. O., ROOSENBOOM, E. W. M., SCHRÖDER, A., GEISLER, R., PALLEK, D., AGOC, J. & NEITZKE, K. 2012 Experimental and numerical investigation of a contra rotating open-rotor flowfield. *J. Aircraft* **49** (6), 1868–1877.

VAN ZANTE, D. E. & ENVIA, E. 2014 Prediction of the aero-acoustic performance of open rotors. In *ASME Turbo Expo, Dusseldorf, Germany, 16–20 June*. *ASME Paper No.* GT2014–26413.

WHITFIELD, C. E., MANI, R. & GLIEBE, P. R. 1990*a* High speed turboprop: aeroacoustic study (counterrotation). Volume I: model development. *NASA CR*185241.

WHITFIELD, C. E., MANI, R. & GLIEBE, P. R. 1990*b* High speed turboprop: aeroacoustic study (counterrotation). Volume II: computer programs. *NASA CR*185242.

YOUNG, R. H. 1951 Contra-rotating axial flow fans. *J. Inst. Heating Ventilating Engng* **18** (187), 448–477.

ZACHARIADIS, A., HALL, C. A. & PARRY, A. B. 2011 Contra-rotating open rotor operation for improved aerodynamics and noise at takeoff. In *ASME Turbo Expo 2011, Vancouver, Canada, 6–10 June*. *ASME Paper* GT2011-45205.

ZHANG, W., WANG, X., JING, X., LIANG, A. & SUN, X. 2017 Three-dimensional analysis of vane sweep effects on fan interaction noise. *J. Sound Vib.* **391**, 73–94.